RESEARCH ARTICLE SUMMARY

DRUG DEVELOPMENT

Kinase-impaired BTK mutations are susceptible to clinical-stage BTK and IKZF1/3 degrader NX-2127

Skye Montoya†, Jessie Bourcier†, Mark Noviski†, Hao Lu†, Meghan C. Thompson, Alexandra Chirino, Jacob Jahn, Anya K. Sondhi, Stefan Gajewski, Ying Siow (May) Tan, Stephanie Yung, Aleksandra Urban, Eric Wang, Cuijuan Han, Xiaoli Mi, Won Jun Kim, Quinlan Sievers, Paul Auger, Hugo Bousquet, Nivetha Brathaban, Brandon Bravo, Melissa Gessner, Cristiana Guiducci, James N. Iuliano, Tim Kane, Ratul Mukerji, Panga Jaipal Reddy, Janine Powers, Mateo Sanchez Garcia de los Rios, Jordan Ye, Carla Barrientos Risso, Daniel Tsai, Gabriel Pardo, Ryan Q. Notti, Alejandro Pardo, Maurizio Affer, Vindhya Nawaratne, Tulasigeri M. Totiger, Camila Pena-Velasquez, Joanna M. Rhodes, Andrew D. Zelenetz, Alvaro Alencar, Lindsey E. Roeker, Sanjoy Mehta, Ralph Garippa, Adam Linley, Rajesh Kumar Soni, Sigrid S. Skånland, Robert J. Brown, Anthony R. Mato, Gwenn M. Hansen*, Omar Abdel-Wahab*, Justin Taylor*

INTRODUCTION: Bruton's tyrosine kinase (BTK) is a nonreceptor kinase in the B cell receptor (BCR) signaling cascade critical for B cell survival. As such, chronic lymphocytic leukemia (CLL) and other B cell cancers are sensitive to inhibition of BTK. Covalent and noncovalent inhibitors of BTK have revolutionized the treatment of these cancers. Therefore, understanding mechanisms by which acquired mutations in BTK confer drug resistance and developing new therapies to overcome resistance are critically important.

RATIONALE: We recently discovered BTK mutations that confer resistance across covalent and noncovalent BTK inhibitors. In this study, we found that a group of these mutants impair BTK kinase activity despite still enabling downstream BCR signaling. We therefore set out to understand the nonenzymatic functions of BTK and explored targeted protein degradation to overcome the oncogenic scaffold function of mutant BTK. This effort included evaluation of BTK degradation in patients with CLL treated in a phase 1 clinical trial of NX-2127, a first-in-class BTK degrader (NCT04830137).

RESULTS: BTK enzymatic activity assays revealed that drug resistance mutations in BTK fall into two distinct groups: kinase proficient and kinase impaired. Immunoprecipitation mass spectrometry of kinase-impaired BTK L528W (Leu^{528}→Trp) revealed a scaffold function of BTK with downstream signaling and survival dependent on surrogate kinases that bind to kinase-impaired BTK proteoforms. To target the nonenzymatic functions of BTK, we developed NX-2127, a heterobifunctional molecule that engages the ubiquitin-proteasome system to simultaneously bind both BTK and the cereblon E3 ubiquitin ligase complex, inducing polyubiquitination and proteasome-dependent degradation of IKZF1/3 and all recurrent drug-resistant forms of mutant BTK. The activity of NX-2127 on BTK degradation was further demonstrated in patients with CLL treated in a phase 1 clinical trial of NX-2127, where >80% BTK degradation was achieved and clinical responses were also seen in 79% of evaluable patients, independent of mutant BTK genotypes.

CONCLUSION: We identified that BTK inhibitor resistance mutations fall into two distinct functional categories. Kinase-impaired BTK mutants disable BTK kinase activity while promoting physical interactions with other kinases to sustain downstream BCR signaling. This scaffold function of BTK was disrupted by NX-2127, a potent BTK degrader, which showed promising responses for patients with relapsed and refractory CLL, independently of mutant BTK functional category. ■

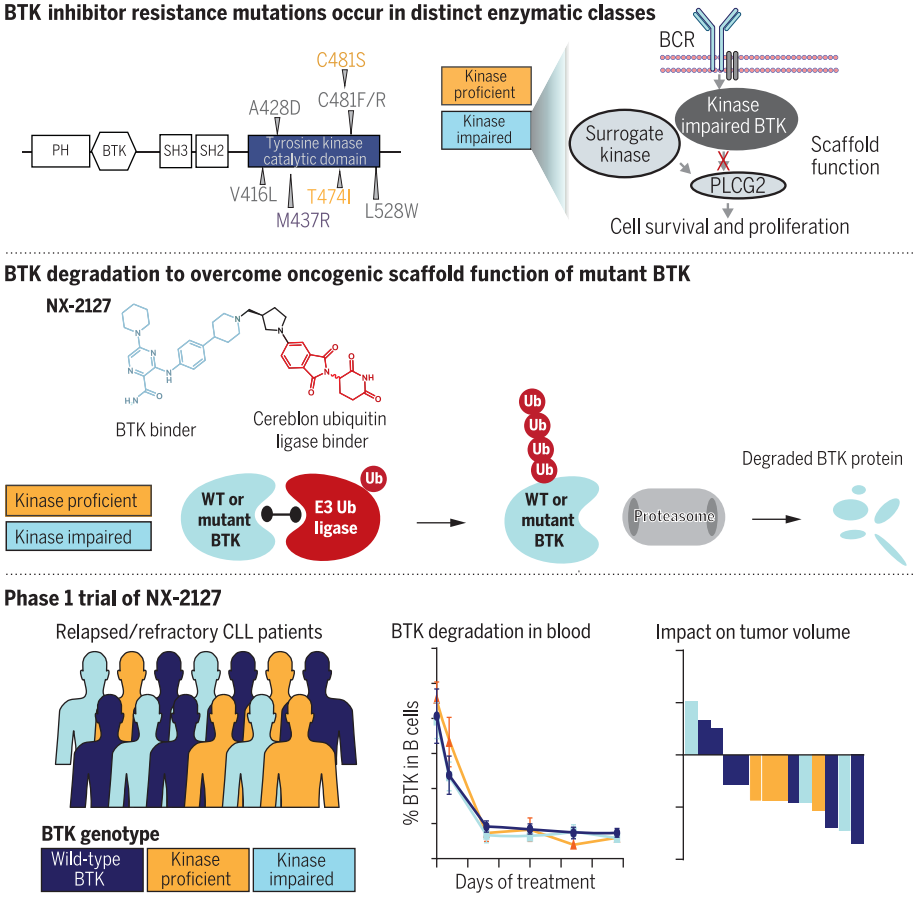

Acquired drug resistance mutations in BTK can diminish BTK's enzymatic activity but are still susceptible to clinical-stage BTK degraders. Acquired mutations that result in resistance to enzymatic BTK inhibitors alter BTK's enzymatic activities, with some mutants being kinase impaired (top). Each recurrent BTK mutant is degraded by a clinical-stage BTK degrader, NX-2127 (middle), which demonstrates BTK degradation and clinical responses in patients with CLL (bottom).

The list of author affiliations is available in the full article online.
*Corresponding author. Email: ghansen@nurixtx.com (G.M.H.); abdelwao@mskcc.org (O.A.-W.); jxt1091@miami.edu (J.T.)
†These authors contributed equally to this work.
Cite this article as S. Montoya *et al.*, *Science* **383**, eadi5798 (2024). DOI: 10.1126/science.adi5798

READ THE FULL ARTICLE AT
https://doi.org/10.1126/science.adi5798

RESEARCH ARTICLE

DRUG DEVELOPMENT

Kinase-impaired BTK mutations are susceptible to clinical-stage BTK and IKZF1/3 degrader NX-2127

Skye Montoya[1]†, Jessie Bourcier[2]†, Mark Noviski[3]†, Hao Lu[3]†, Meghan C. Thompson[4], Alexandra Chirino[1], Jacob Jahn[1], Anya K. Sondhi[1], Stefan Gajewski[3], Ying Siow (May) Tan[3], Stephanie Yung[3], Aleksandra Urban[5,6], Eric Wang[7], Cuijuan Han[7], Xiaoli Mi[2], Won Jun Kim[2], Quinlan Sievers[2], Paul Auger[3], Hugo Bousquet[3], Nivetha Brathaban[3], Brandon Bravo[3], Melissa Gessner[3], Cristiana Guiducci[3], James N. Iuliano[3], Tim Kane[3], Ratul Mukerji[3], Panga Jaipal Reddy[3], Janine Powers[3], Mateo Sanchez Garcia de los Rios[3], Jordan Ye[3], Carla Barrientos Risso[1], Daniel Tsai[1], Gabriel Pardo[1], Ryan Q. Notti[8], Alejandro Pardo[1], Maurizio Affer[1], Vindhya Nawaratne[1], Tulasigeri M. Totiger[1], Camila Pena-Velasquez[2], Joanna M. Rhodes[9], Andrew D. Zelenetz[10], Alvaro Alencar[1], Lindsey E. Roeker[2], Sanjoy Mehta[11], Ralph Garippa[11], Adam Linley[12], Rajesh Kumar Soni[13], Sigrid S. Skånland[2,5,6], Robert J. Brown[3], Anthony R. Mato[2], Gwenn M. Hansen[3]*, Omar Abdel-Wahab[2]*, Justin Taylor[1]*

Increasing use of covalent and noncovalent inhibitors of Bruton's tyrosine kinase (BTK) has elucidated a series of acquired drug-resistant BTK mutations in patients with B cell malignancies. Here we identify inhibitor resistance mutations in BTK with distinct enzymatic activities, including some that impair BTK enzymatic activity while imparting novel protein-protein interactions that sustain B cell receptor (BCR) signaling. Furthermore, we describe a clinical-stage BTK and IKZF1/3 degrader, NX-2127, that can bind and proteasomally degrade each mutant BTK proteoform, resulting in potent blockade of BCR signaling. Treatment of chronic lymphocytic leukemia with NX-2127 achieves >80% degradation of BTK in patients and demonstrates proof-of-concept therapeutic benefit. These data reveal an oncogenic scaffold function of mutant BTK that confers resistance across clinically approved BTK inhibitors but is overcome by BTK degradation in patients.

Bruton's tyrosine kinase (BTK) is a central mediator of B cell activation, proliferation, and signaling downstream of the B cell receptor (BCR), making it a key target for B cell neoplasms (*1*–*3*). BTK inhibitors have changed the treatment landscape of the B cell malignancies chronic lymphocytic leukemia (CLL), mantle cell lymphoma (MCL), and Waldenström macroglobulinemia (*1*, *4*–*7*). Covalent BTK inhibitors (ibrutinib, acalabrutinib, and zanubrutinib) irreversibly bind BTK at cysteine 481 (C481) and prevent BTK autophosphorylation at tyrosine 223 (Y223) as well as phosphorylation of BTK's downstream substrates (*4*, *8*–*10*).

Despite excellent clinical outcomes for patients treated with covalent BTK inhibitors, acquired resistance to covalent BTK inhibitors are a limitation of their clinical use. Specifically, acquired mutations at the C481 residue of BTK confer resistance to all covalent BTK inhibitors (*11*–*14*). Noncovalent inhibitors of BTK do not require C481 to bind and can overcome C481 mutant–mediated resistance (*5*, *15*, *16*). Two such inhibitors, pirtobrutinib and nemtabrutinib, are currently under evaluation in clinical trials, with early results showing an overall response rate of 74% for pirtobrutinib and 56% for nemtabrutinib in relapsed/refractory CLL patients as single agents (*5*, *17*, *18*). In 2023, on the basis of clinical activity and safety demonstrated in the phase 1/2 BRUIN trial, pirtobrutinib was approved by the US Food and Drug Administration (FDA) for patients with MCL after at least two lines of therapy, including a prior covalent BTK inhibitor, and for patients with CLL after at least two lines of therapy, including a prior covalent BTK inhibitor and a BCL-2 inhibitor.

Although both covalent and noncovalent BTK inhibitors offer therapeutic benefits, it is now clear that acquired mutations in BTK outside of the C481 residue can confer resistance to noncovalent inhibitors and that a portion of these mutations also cause cross-resistance to certain covalent BTK inhibitors (*5*, *19*–*22*). Surprisingly, some BTK drug resistance mutations appear to reduce BTK Y223 autophosphorylation (*5*). This is an unexpected finding, as BTK Y223 phosphorylation is required for BTK's phosphorylation of downstream substrates to sustain BCR signaling (*23*, *24*). A scaffold function of BTK, independent of its catalytic activity, has long been suspected. For example, mice bearing experimental Y223F (Tyr^{223}→Phe) BTK mutations that prevent BTK autophosphorylation or experimental kinase-inactivating K430R mutations have been shown to still develop peripheral B cells, a phenotype not seen with complete BTK deletion (*25*). Despite these findings, a precise function of BTK independent of its kinase activity has not been well elucidated.

In this study, we identified that recurrent BTK mutations that cause resistance to covalent and/or noncovalent BTK inhibitors occur in two distinct enzymatic groups: certain BTK mutations are kinase proficient (T474I/F and C481S), whereas others greatly reduce BTK enzymatic function (M437R, V416L, C481Y/R/F, and L528W). We used several orthogonal unbiased proteomic approaches to demonstrate that, despite their diminished catalytic activity, these kinase-impaired mutant versions of BTK maintain signaling downstream of the BCR through enhanced physical interactions and activation of multiple signaling moieties in malignant B cells. Furthermore, we identified that the scaffold function activity of BTK, which does not rely on BTK enzymatic activity, can be overcome in patients by a novel clinical-stage BTK degrader, NX-2127. Whereas several proteolysis-targeting chimera (PROTAC) degraders of BTK have been demonstrated to target BTK wild-type (WT) or C481S-mutant forms of BTK in preclinical studies (*26*–*28*), we now demonstrate degradation of each drug-resistant BTK proteoform as well as BTK degradation in the blood of CLL patients bearing these mutations treated on a phase 1, first-in-human clinical trial of NX-2127 (NCT04830137).

Drug resistance mutations in BTK have distinct enzymatic activities with differential BCR signaling activation

We recently identified that certain drug resistance mutations in BTK are associated with reduced autophosphorylation of BTK at Y223 (*5*). Additionally, publications by Dhami *et al.* and Yuan *et al.* identified that BTK C481F/Y and L528W mutations, respectively, are associated

[1]Sylvester Comprehensive Cancer Center, University of Miami Miller School of Medicine, Miami, FL, USA. [2]Molecular Pharmacology Program, Sloan Kettering Institute, Memorial Sloan Kettering Cancer Center, New York, NY, USA. [3]Nurix Therapeutics, San Francisco, CA, USA. [4]Leukemia Service, Department of Medicine, Memorial Sloan Kettering Cancer Center, New York, NY, USA. [5]Department of Cancer Immunology, Institute for Cancer Research, Oslo University Hospital, Oslo, Norway. [6]K.G. Jebsen Centre for B Cell Malignancies, Institute of Clinical Medicine, University of Oslo, Oslo, Norway. [7]The Jackson Laboratory for Genomic Medicine, Farmington, CT, USA. [8]Laboratory of Molecular Electron Microscopy, Rockefeller University, New York, NY, USA. [9]Division of Hematology-Oncology, Department of Medicine at Zucker School of Medicine at Hofstra/Northwell, CLL Research and Treatment Center, Lake Success, NY, USA. [10]Lymphoma Service, Department of Medicine, Memorial Sloan Kettering Cancer Center, New York, NY, USA. [11]Gene Editing and Screening Core Facility, Department of Cancer Biology and Genetics, Memorial Sloan Kettering Institute and Cancer Center, New York, NY, USA. [12]Department of Molecular and Clinical Cancer Medicine, Institute of Systems, Molecular and Integrative Biology, University of Liverpool, Liverpool, UK. [13]Proteomics and Macromolecular Crystallography Shared Resource, Herbert Irving Comprehensive Cancer Center, Columbia University, New York, NY, USA.
*Corresponding author. Email: ghansen@nurixtx.com (G.M.H.); abdelwao@mskcc.org (O.A.-W.); jxt1091@miami.edu (J.T.)
†These authors contributed equally to this work.

with reduced BTK enzymatic activity (*29*, *30*). To comprehensively evaluate the enzymatic activity and signaling properties of B cells with each recurrent BTK drug resistance mutation, we first expressed BTK WT, V416L, A428D, M437R, T474I, C481S, or L528W mutants or a negative empty vector control in BTK null DT40 chicken B lymphocytes. Western blot analyses evealed clear reductions in phospho-BTK (p-BTK) Y223 in V416L, A428D, M437R, and L528W mutant cells relative to BTK WT (fig. S1, A and B). To evaluate BTK enzymatic activity at physiological levels of BTK expressed from the endogenous BTK locus, we generated TMD8 cells (a human BTK-dependent diffuse large B cell lymphoma cell line) with knock-in BTK V416L, T474I, and L528W mutations. Of note, TMD8 cells were established from a male patient, and we confirmed that each mutation was successfully introduced into the single X-linked BTK allele (fig. S1C). Evaluation of p-BTK Y223 in this series of knock-in cell lines revealed stark decreases in p-BTK Y223 in BTK V416L and L528W lines compared with BTK WT cells in the presence or absence of BCR stimulation with anti–immunoglobulin M (IgM) (Fig. 1A). Conversely, BTK T474I cells had increased p-BTK Y223 compared with BTK WT cells, which was evident even before BCR stimulation. Similar findings were seen without BCR cross-linking in the presence or absence of treatment with the noncovalent BTK inhibitor pirtobrutinib (fig. S1D).

Given the above results, activities of full-length recombinant BTK WT and eight distinct drug resistant mutants (V416L, A428D, M437R, T474I, C481S, C481F, C481R, and L528W) were assessed in an ADP-Glo assay. Measurement of the ability of WT versus mutant BTK proteins to hydrolyze a fixed concentration of adenosine triphosphate (ATP) revealed significantly reduced enzymatic activity of BTK V416L, A428D, M437R, C481F, C481R, and L528W mutants compared with WT BTK. Conversely, BTK T474I and C481S mutants were intact in their ability to hydrolyze ATP (fig. S1E). To quantitatively determine kinase activity, a fluorescence resonance energy transfer (FRET) assay that measures specific signal upon tyrosine phosphorylation of a peptide substrate was developed. Determining the rate of phosphorylation at a range of ATP concentrations confirmed that these mutants have distinct kinase activities. BTK C481S, a resistance mutation common to all covalent inhibitors, does not significantly affect catalytic activity of BTK [as measured by ATP K_m (Michaelis-Menten constant) and overall catalytic efficiency (k_{cat}/K_m, ATP)]. In contrast, the BTK T474I mutant showed reduced ATP K_m and increased k_{cat}, yielding an 18-fold increase of catalytic efficiency compared with WT. At the same time, the BTK M437R mutant retains only 11% catalytic activity compared with WT BTK, while the BTK V416L and L528W mutant proteins are <1% active (Fig. 1, B and C, and fig. S1F). Overall, the results of our cellular and cell-free measurements of BTK enzymatic activity reveal that drug resistance mutations in BTK fall into two distinct groups: kinase proficient (T474I and C481S) and kinase impaired (M437R, V416L, L528W, C481F, C481Y, and C481R) (Fig. 1D).

The discovery that certain BTK mutants have impaired kinase function is surprising, as TMD8 cells and CLL cells are dependent on the presence of BTK for cell survival (*29*, *31*). These findings therefore suggest that kinase-disabling mutations in BTK may engender novel functions, distinct from the consequences of complete elimination of BTK protein. To understand how BCR signaling is affected by mutations such as BTK L528W that impair kinase function, we next used a kinobead/mass spectrometry–based protocol to systematically evaluate the abundance of kinases and their active site availability in BTK WT and mutant TMD8 cells. Recently, this approach was successfully used to probe BCR signaling in CLL cells (*32*) and was performed here with and without IgM stimulation and in the presence or absence of pirtobrutinib treatment (fig. S1G). Lysates from BTK WT or L528W mutant cells were incubated with kinobeads bound to CTx-0294885, a broad-spectrum kinase inhibitor that captures members of all kinase subfamilies, including well-characterized BCR signalosome proteins such as LYN, SYK, and BTK (*33*). Pirtobrutinib treatment failed to down-regulate the increased expression of BCR signaling components (such as SYK, LYN, and HCK) in BTK L528W mutant cells in response to IgM stimulation (fig. S1, H and I).

In addition to the kinobead assay, we also measured calcium ion (Ca^{2+}) flux, a pathway dependent on BCR activity in B cells. Consistent with the kinobead/mass spectrometry results, TMD8 cells overexpressing kinase impaired (M437R, V416L, and L528W) BTK mutations showed increased Ca^{2+} flux in response to IgM stimulation compared with WT BTK, despite their greatly reduced catalytic activity (Fig. 1E and fig. S1J).

To systematically evaluate tyrosine-phosphorylated substrates in TMD8 cells bearing WT versus kinase-proficient (BTK T474I) and kinase-impaired (BTK L528W) mutations, we next performed unbiased phosphoproteomics with phosphotyrosine enrichment (fig. S2, A and B). Consistent with Western blot data and in vitro enzymatic assays, phosphoproteomics revealed increased phosphorylation of BTK across identified tyrosine sites (Y223, Y461, and Y551) in T474I mutant cells yet reduced BTK phosphorylation in L528W mutant cells relative to WT (Fig. 1, F and G). Beyond BTK phosphorylation, up-regulation of tyrosine phosphorylation in the predicted substrates of kinases in the MAPK (mitogen-activated protein kinase) and SRC families specific to the L528W mutant was seen using kinase substrate enrichment analysis (KSEA) (Fig. 1H). These data provide further evidence of an alternative signaling mechanism in BTK kinase-impaired mutant cells.

BTK mutations with impaired kinase activity confer novel BTK protein interactions

Given persistence of BCR signaling downstream of mutant BTK regardless of the level of observable enzymatic activity, we hypothesized the existence of a novel scaffold function of BTK. To unbiasedly identify interactors of the kinase-impaired BTK L528W mutant, we performed immunoprecipitation (IP) of BTK in TMD8 cells overexpressing 3X FLAG-tagged BTK WT or L528W followed by mass spectrometry. We identified a number of proteins uniquely interacting with BTK L528W compared with WT BTK in the presence or absence of BCR stimulation with IgM (Fig. 2A). To validate our mass spectrometry findings by orthogonal method, we performed two-dimensional difference gel electrophoresis (2D DIGE) analyses followed by quantitative protein identification of proteins immunoprecipitated from BTK in the knock-in TMD8 cell lines (fig. S2, C to E). Results from three biological replicates showed 46 differentially expressed protein spots between WT and mutant BTK, which were then identified by mass spectrometry. Of these, 31 were significantly up-regulated in the L528W mutant relative to WT, and 11 were also found in the direct BTK IP/mass spectrometry experiments (Fig. 2B and fig. S2E). Of particular interest, IP of BTK WT or mutant forms in knock-in cells followed by Western blot analysis confirmed distinct interactions of BTK L528W with HCK (hematopoietic cell kinase) and ILK (integrin-linked kinase) (Fig. 2C).

HCK is a member of the SRC-family tyrosine kinases predominantly expressed in the hematopoietic lineage and known to play a role in the survival of a number of hematologic and solid malignancies (*34*). Notably, recent work has identified that kinase-impaired C481 BTK mutants physically interact with HCK and dysregulate the autoinhibitory loop of HCK, allowing HCK to propagate downstream BCR signaling (*29*). Here, our data suggest that the BTK mutant–HCK interaction also extends to BTK L528W mutation while also identifying that kinase-impaired BTK mutants have a broader range of interacting proteins other than just HCK. One such example is ILK, a serine/threonine kinase commonly up-regulated in malignant cells. Emerging evidence demonstrates an important role for ILK in tumorigenesis, cancer cell proliferation, and drug resistance (*35*, *36*). ILK can also phosphorylate AKT on serine 473 and is sensitive to PIP3

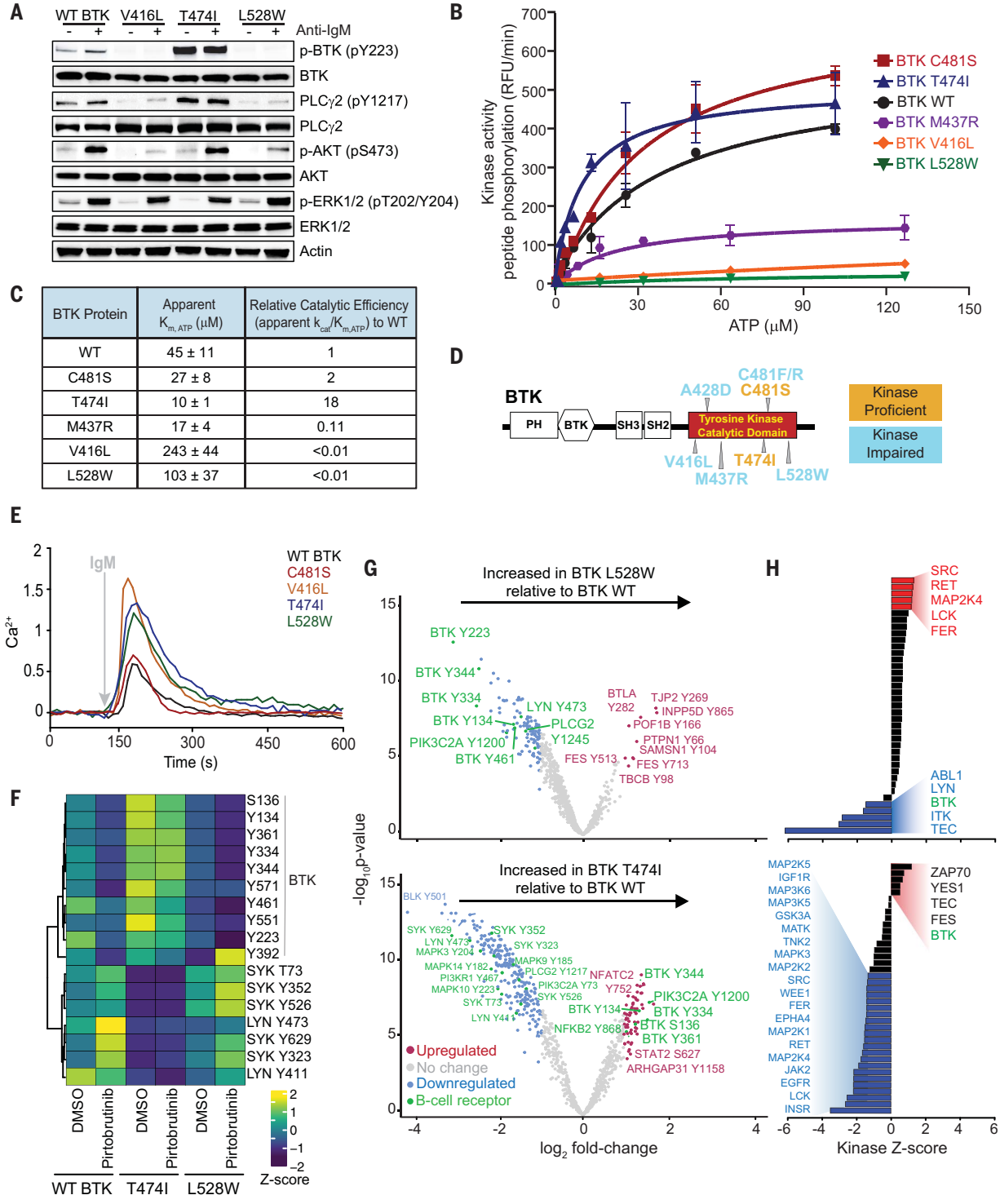

BTK Protein	Apparent $K_{m,ATP}$ (μM)	Relative Catalytic Efficiency (apparent $k_{cat}/K_{m,ATP}$) to WT
WT	45 ± 11	1
C481S	27 ± 8	2
T474I	10 ± 1	18
M437R	17 ± 4	0.11
V416L	243 ± 44	<0.01
L528W	103 ± 37	<0.01

Fig. 1. Drug-resistant mutations in BTK occur in distinct enzymatic classes, and kinase-impaired forms of BTK have sustained B cell receptor signaling. (**A**) Western blot analysis of downstream signaling in TMD8 cells with WT or knock-in of mutant BTK V416L, T474I, and L528W in the absence or presence of IgM stimulation. (**B**) Michaelis-Menten plots of the kinase activities of BTK WT and mutants. Kinase activities were measured using signal from tyrosine phosphorylation of a peptide substrate at a range of ATP concentrations in a FRET assay. For BTK M437R, V416L, and L528W, higher ATP concentrations were tested (500 μM). (**C**) Table showing apparent Michaelis-Menten constant of ATP required to yield a signal ($K_{m,ATP}$) and relative catalytic efficiency (k_{cat}/K_m) of each BTK mutant purified protein within a 60-min range from the FRET-based kinase activity assay. Each value is the mean ± SD of three experiments. (**D**) Diagram of drug-resistant mutations in BTK and their impact on BTK enzymatic activity. (**E**) Measurements of intracellular calcium (Ca^{2+}) release upon IgM-mediated cross-linking of the BCR over time in TMD8 cells overexpressing WT or mutant BTK. (**F**) Heatmap of phosphorylation of BTK, SYK, and LYN at the indicated amino acid residues in BTK WT, T474I, and L528W mutant cells in the presence or absence of pirtobrutinib treatment (1 μM for 1 hour). (**G**) Volcano plots of differentially phosphorylated peptides in BTK L528W versus WT BTK (top) or BTK T474I versus WT BTK (bottom) cells. Samples were prepared in triplicate and

analyzed after phosphotyrosine enrichment using TMT mass spectrometry with an FDR adjusted significance threshold of $P < 0.05$. (**H**) Kinase substrate enrichment analysis showing predicted alterations in protein kinase–mediated signaling on the basis of hypo- or hyperphosphorylated substrates from (G), highlighting significantly active (red) and significantly inactive (blue) genes in BTK L528W versus WT BTK (top) or BTK T474I versus WT BTK (bottom) expressing cells. Single-letter abbreviations for the amino acid residues are as follows: A, Ala; C, Cys; D, Asp; E, Glu; F, Phe; G, Gly; H, His; I, Ile; K, Lys; L, Leu; M, Met; N, Asn; P, Pro; Q, Gln; R, Arg; S, Ser; T, Thr; V, Val; W, Trp; and Y, Tyr.

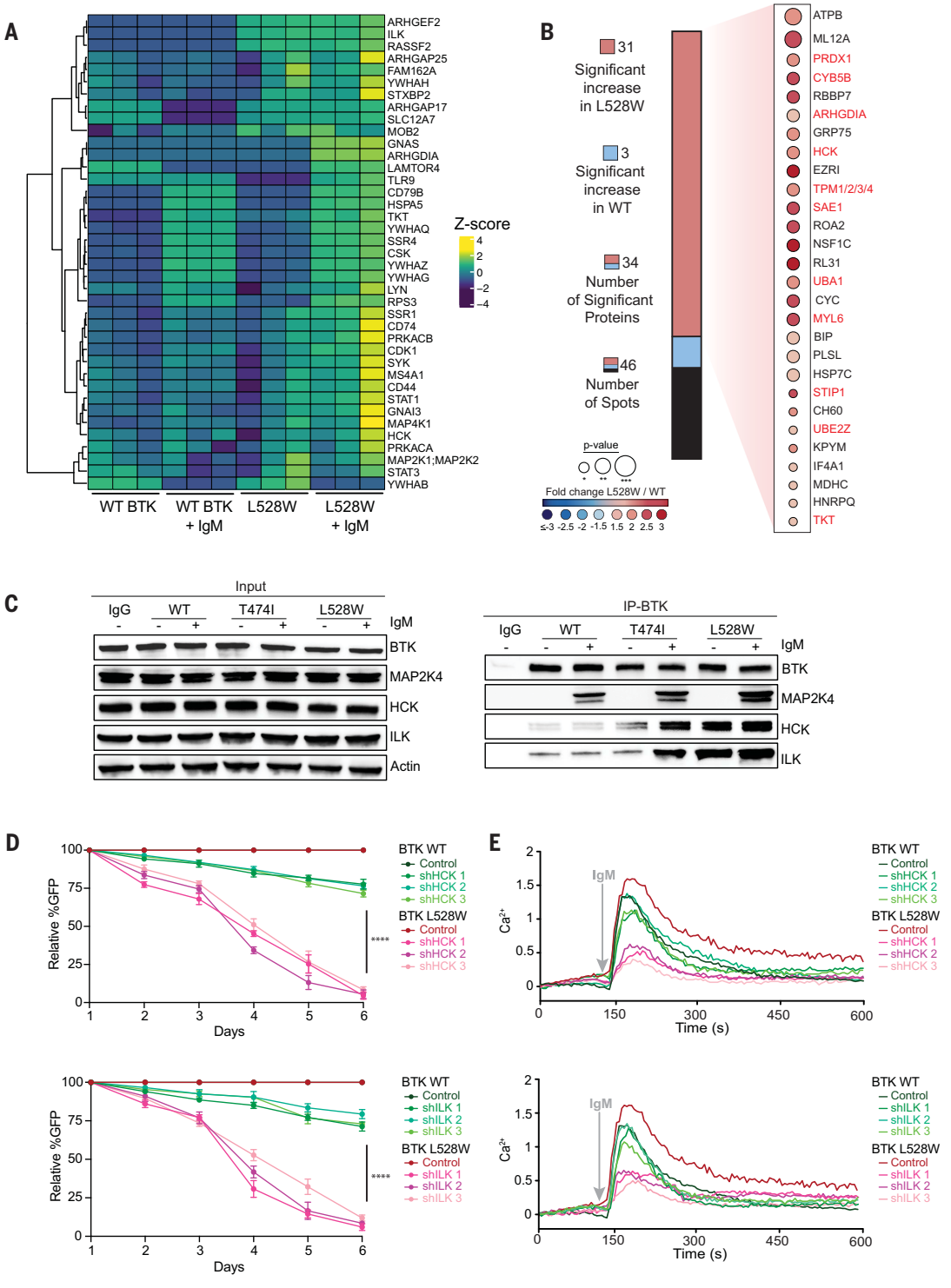

Fig. 2. Kinase-impaired BTK mutations enhance interaction with additional signaling proteins downstream of the BCR and discovery of the immunomodulatory drug–based BTK degrader NX-2127. (**A**) Heatmap of signaling proteins identified from IP mass spectrometry interacting with 3X FLAG-tagged WT or mutant BTK in TMD8 cells in the absence or presence of IgM stimulation. (**B**) Stacked bar chart illustrating results from 2D DIGE gel analysis and protein identification after BTK immunoprecipitation from knock-in TMD8 cell lines. Proteins significantly up-regulated in L528W mutant highlighted in dot plot with proteins also seen in IP mass spectrometry experiment in red text. (**C**) Western blot analysis in knock-in TMD8 cells after immunoprecipitation of endogenous WT or mutant BTK in the presence or absence of IgM stimulation. (**D**) Relative GFP expression over a 6-day period in TMD8 BTK WT or BTK L528W knock-in cells after doxycycline induction of tetracycline-inducible HCK knockdown (shHCK 1, shHCK 2, or shHCK 3), ILK knockdown (shILK 1, shILK 2, or shILK 3) or nontargeted control vector. (**E**) Measurements of intracellular calcium (Ca^{2+}) release upon IgM-mediated cross-linking of the BCR over time in TMD8 BTK WT or BTK L528W knock-in cells after 48-hour doxycycline induction of HCK or ILK knockdown. All Western blots are representative of three independent experiments. Nonlinear mixed model was used to analyze data in (D). Data in (D) represent data + SEM from $n = 3$ replicates. ****$P < 0.0001$.

(phosphatidylinositol 3,4,5-trisphosphate) levels in cells (*37*, *38*).

We functionally evaluated the potential requirement of HCK and ILK for survival and downstream BCR signaling in BTK mutant relative to BTK WT cells. We generated BTK L528W and BTK WT cells with stable expression of an inducible construct that allows for induction of green fluorescent protein (GFP) along with short hairpin RNAs (shRNAs) targeting HCK, ILK, or a nontargeting control shRNA. Once successful knockdown of HCK and ILK was confirmed upon doxycycline induction in these cells (fig. S2F), we evaluated the impact of HCK and ILK on the growth and BCR signaling in BTK WT versus L528W mutant cells by competition assay and calcium release upon IgM stimulation, respectively. These assays both demonstrated that BTK L528W mutant cells were preferentially dependent on either HCK or ILK for cell proliferation and BCR signaling compared with BTK WT cells (Fig. 2, D and E).

Taken together, the aforementioned data demonstrate that BTK mutants that confer resistance to BTK inhibitors by impairing BTK enzymatic activity achieve this effect by simultaneously enhancing the physical interactions of BTK with signaling molecules such as HCK and ILK. This process bypasses the requirement for BTK phosphorylation at tyrosine 223 to confer and sustain downstream BCR signaling.

Development of NX-2127, a clinical-grade orally bioavailable BTK and IKZF1/3 degrader

Given that BTK covalent and noncovalent drug resistance mutations do not rely on kinase activity, we next investigated a means to eliminate, rather than enzymatically inhibit, mutant BTK proteins. Unlike small-molecule inhibitors, targeted protein degraders take advantage of the cell's innate machinery for protein regulation to catalytically degrade rather than enzymatically inhibit proteins. This modality enables greater drug selectivity and longer-lasting pharmacological effects owing to the requirement for cells to synthesize new protein in order to recover activity (*38*, *39*).

To generate a BTK degrader, several high-affinity BTK binders (hook) were surveyed for their ability to degrade BTK in Ramos cells when coupled to an imide-based cereblon (CRBN) ligand with flexible polyethylene glycol or alkyl linkers of various lengths. This initial matrix of bifunctional compounds yielded several potent hits that were then further optimized through structure-based drug design, medicinal chemistry optimization, and in vitro and in vivo empirical testing to ultimately identify a potent, selective, and orally bioavailable BTK degrader, NX-2127 (Fig. 3A). This heterobifunctional molecule can efficiently engage the intracellular ubiquitin-proteasome system to simultaneously bind both BTK and the CRBN E3 ubiquitin ligase complex, inducing polyubiquitination and proteasome-dependent degradation of BTK, IKZF1, and IKZF3.

Ikaros (IKZF1) and Aiolos (IKZF3) are key lymphocyte transcription factors that directly suppress cytokines such as interleukin-2 (IL-2) and are implicated in B cell, T cell, and natural killer cell proliferation and activation (*40*–*43*). Lenalidomide, an imide-containing immunomodulatory drug, has been approved by the FDA to treat various B cell malignancies including MCL, multiple myeloma, myelodysplastic syndromes associated with a deletion 5q, follicular lymphoma, and marginal zone lymphoma (*44*). Moreover, in diffuse large B cell lymphoma (DLBCL), this drug has demonstrated direct tumor killing and has been used in a combination therapy with ibrutinib and rituximab showing promising efficacy, especially in the non–germinal center type (*45*).

NX-2127 binds to recurrent acquired resistant forms of mutant BTK

We next used a FRET-based probe displacement assay to measure the binding affinity of ibrutinib, pirtobrutinib, and NX-2127 (BTK degrader) to full-length recombinant BTK proteins (WT and mutants). This revealed impaired binding to BTK mutants relative to WT for both ibrutinib (C481S and L528W) and pirtobrutinib (T474I, M437R, V416L, and L528W). The BTK L528W mutation, which confers resistance to both ibrutinib and pirtobrutinib, completely abolished binding of either drug to BTK [half-maximal inhibitory concentration (IC_{50}) >1000 nM]. Despite a relatively weaker binding affinity to WT BTK (IC_{50} = 10 nM) compared with enzymatic BTK inhibitors, NX-2127 bound all recurrent drug-resistant forms of BTK (Fig. 3, B and C). Surface plasmon resonance (SPR) was used to measure the dissociation constant (K_d) of NX-2127. The degrader exhibited rapid association and dissociation rates, with K_d values of 18 nM (for WT BTK), 45 nM (BTK C481S), 18 nM (BTK T474I), 44 nM (BTK M437R), 97 nM (BTK V416L), and 88 nM (BTK L528W) (Fig. 3C and fig. S3, A to D).

NX-2127 induces stable ternary complex formation between BTK proteoforms and the E3 ubiquitin ligase CRBN/DDB1 complex

Favorable interactions between an E3 ligase and the target protein induced by a degrader can lead to potent and selective degradation (*46*, *47*). We used a nano bioluminescence resonance energy transfer (NanoBRET) assay to confirm that NX-2127 induces dose-dependent ternary complex formation between CRBN and WT or mutant BTK in cells (Fig. 3D). To determine the cooperativity of ternary complexes induced by NX-2127, we used a FRET-based probe displacement assay and measured BTK-binding IC_{50} values without and with saturating CRBN/DDB1 (DNA damage-binding protein 1) complex. These results revealed positive cooperativity (α) in ternary complex with BTK WT (α = 2.2) and the BTK mutants C481S (α = 3.0), T474I (α = 3.1), M437R (α = 2.7), V416L (α = 3.0), and L528W (α = 3.7) (Fig. 3, E and F, and fig. S3E).

Together, data from our FRET, SPR, and NanoBRET assays revealed that the binding affinity of NX-2127 to BTK was relatively uninfluenced by mutations that cause resistance to covalent and noncovalent BTK inhibitors. These data emphasize the potential of such a degrader strategy to overcome BTK mutations that engender resistance to multiple classes of enzymatic inhibitors.

Crystal structure of NX-2127 hook bound to BTK WT and L528W kinase domain

We next sought to determine the structural basis for the observed reduction of catalytic activity in BTK L528W as well as the maintenance of NX-2127 binding to mutant BTK. To do this, we generated the crystal structures of BTK WT and L528W mutant kinase domains bound to the hook portion of NX-2127 (Fig. 4A and table S1) at 1.9-Å and 1.75-Å resolution, respectively. The major interaction between BTK and NX-2127 originates in the hydrogen bond donor-acceptor motif from the ligand amide to the backbone carbonyl of E475 and amide nitrogen of M477 in the hinge region of BTK (fig. S4A). In the WT structure, the binding interaction of the ligand closely matches interactions reported for precursor degrader NRX-0492 (*28*), demonstrating that binding of this scaffold to BTK is not affected by the oxoimidazolidine moiety (fig. S4A). The binding pose of the NX-2127 hook reveals that there is large unoccupied space between the ligand and the mutated T474, C481, and M437 residues, which are quite distant from each other. Specifically, the distance of the Cβ atom of each respective residue to the closest heavy atom in the ligand is 4.8 Å for T474, 4.4 Å for C481, and 14.7 Å for M437 (fig. S4B), potentially explaining why binding affinities of NX-2127 are not substantially affected by mutations at these residues.

BTK inhibitor resistance mutations also occur at amino acids V416, A428, and L528. These residues are part of the hydrophobic motif named the catalytic (C)–spine which is assembled upon ATP binding and is important for catalysis (*48*). Results from kinase activity assays revealed that resistance mutations V416L, A428D, and L528W lead to significantly lower kinase activity. In the L528W mutant structure, NX-2127 binds similarly to what was observed in ligand-bound WT structure. However, steric repulsion by the tryptophan side chain and the piperidine moiety forces the ligand to move ~18° toward the BTK P-loop and wedges the N-lobe away from the C-lobe (Fig. 4A). The

A

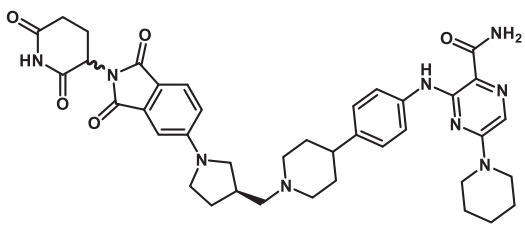

NX-2127
molecular weight = 719.85
calculated partition coefficient (cLogP) = 3.63
pKa = 8.03

B

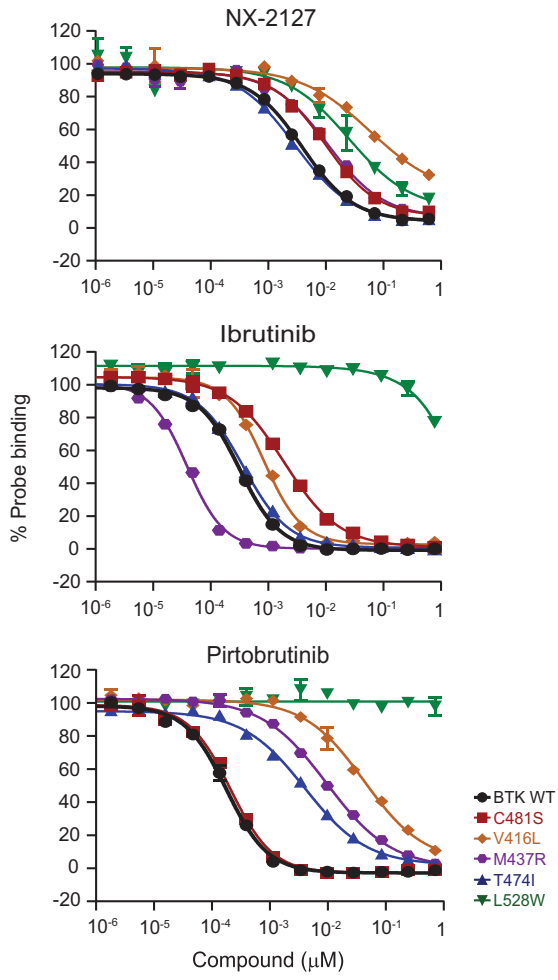

C

BTK Protein	Binding Affinity of NX-2127 Determined by SPR K_d (nM)	Binding Determined by FRET Displacement Assay		
		NX-2127 (Degrader) IC_{50} (nM)	Pirtobrutinib (non-covalent inhibitor) IC_{50} (nM)	Ibrutinib (covalent inhibitor) IC_{50} (nM)
WT	18 ± 3	10 ± 1	0.76 ± 0.19	1.4 ± 0.1
C481S	45 ± 11	22 ± 2	0.77 ± 0.16	6.2 ± 0.3
T474I	18 ± 3	8.6 ± 0.8	12 ± 2	1.8 ± 0.3
M437R	44 ± 11	23 ± 2	30 ± 5	0.28 ± 0.07
V416L	97 ± 10	165 ± 18	98 ± 8	3.8 ± 0.7
L528W	88 ± 3	70 ± 10	>1000	>1000

D

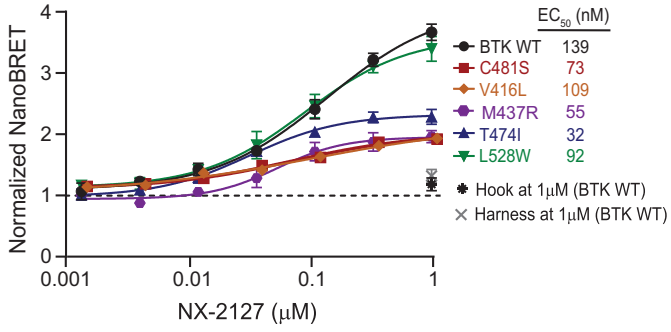

E

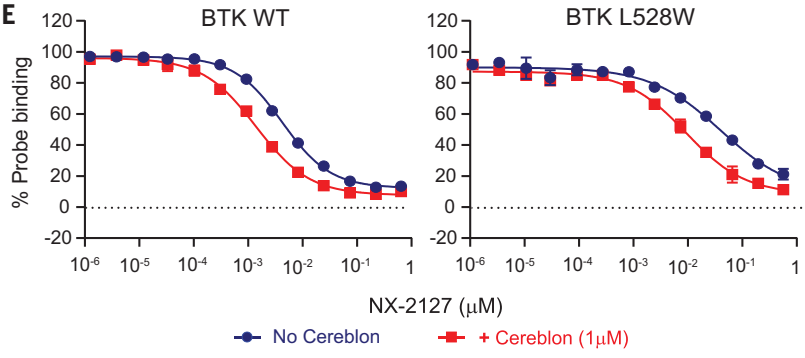

F

BTK Protein	IC_{50} (nM) without CRBN	IC_{50} (nM) with 1μM CRBN	Cooperativity (α)
WT	10 ± 1	4.7 ± 1.5	2.2
C481S	22 ± 2	7.5 ± 1.8	3.0
T474I	8.6 ± 0.8	2.8 ± 0.7	3.1
M437R	23 ± 2	8.7 ± 3.2	2.7
V416L	165 ± 18	55 ± 8	3.0
L528W	70 ± 10	19 ± 5	3.7

Fig. 3. NX-2127 binds to all classes of drug-resistant BTK mutant proteins and induces stable ternary complex formation with CRBN-DDB1 E2 ubiquitin ligase and BTK. (**A**) Chemical structure and properties of NX-2127. (**B**) Binding curves of NX-2127 (top), ibrutinib (middle), and pirtobrutinib (bottom) to full-length BTK WT and mutant proteins in a FRET probe displacement assay. For ibrutinib, binding to BTK proteins was measured kinetically without preincubating compound and protein. Curves and IC_{50} values represent binding at steady state at 60 min. For NX-2127 and pirtobrutinib, compound and protein were incubated for 120 min, and binding curves and IC_{50} values were determined using an end-point readout. (**C**) Dissociation constants (K_d) of NX-2127 determined by SPR and IC_{50} of NX-2127, pirtobrutinib, and ibrutinib measured in the FRET probe displacement assay. Each value is the mean ± SD of three or more experiments. (**D**) Ternary complex formation in human embryonic kidney 293 cells coexpressing NanoLuc BTK WT or mutant and Halo-tag cereblon. The assay was performed with a range of NX-2127 concentrations. Data represent normalized NanoBRET signal to DMSO after 6-hour treatment in technical triplicate. (**E**) Binding of NX-2127 to BTK WT (left) and L528W (right) in the absence and presence of saturating CRBN/DDB1 (1 μM) complex to determine cooperativity using the FRET probe displacement assay. (**F**) Cooperativity values of different ternary complexes between full-length BTK (WT and mutants) and CRBN/DDB1 induced by NX-2127. Each IC_{50} value is the mean ± SD of three experiments. Cooperativity was calculated from the ratio of averaged IC_{50} without and with saturating CRBN/DDB1 complex. Data in (B) and (F) represent average values + SD from n = 3 or more independent experiments.

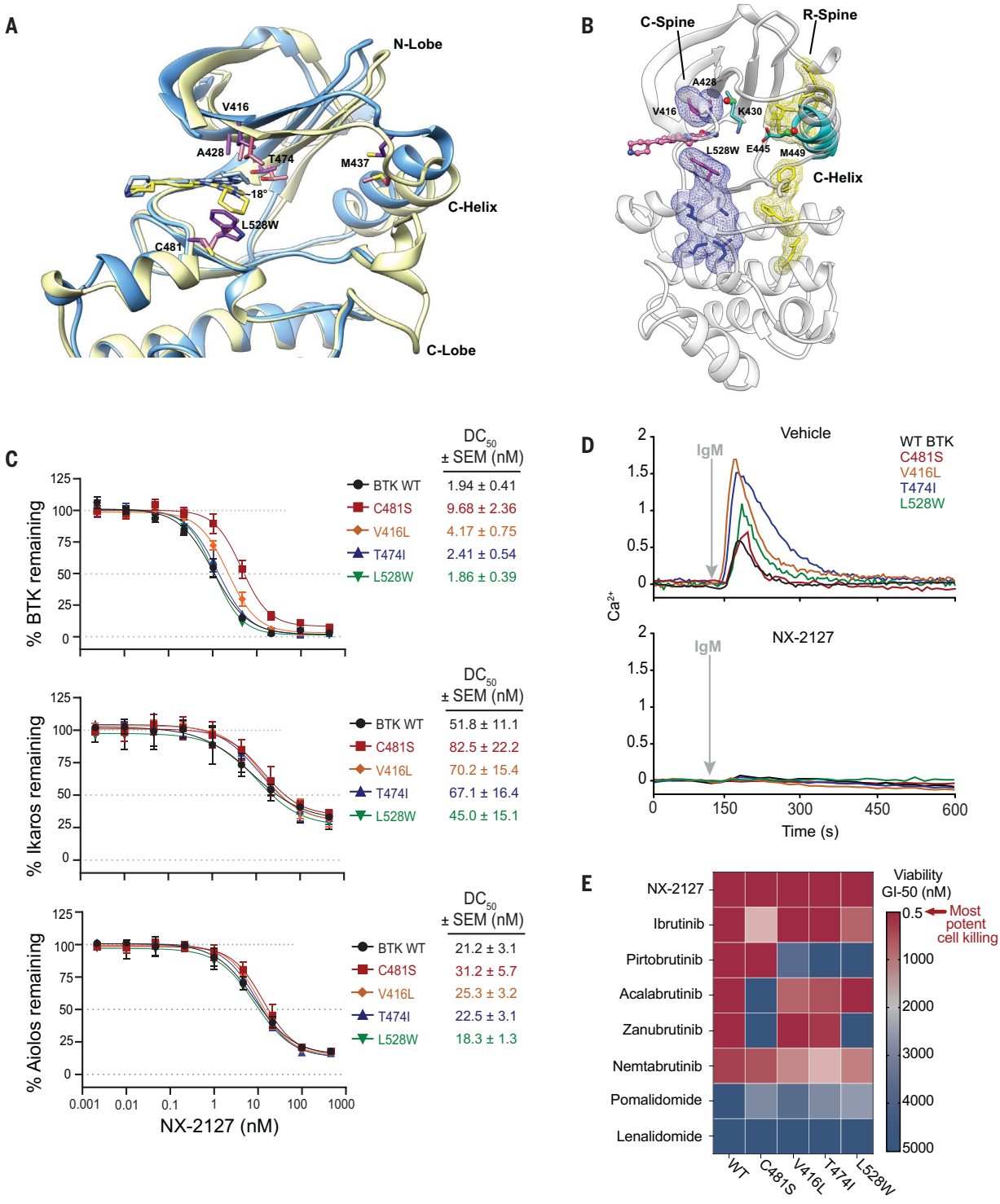

Fig. 4. NX-2127 degrades BTK drug-resistant mutant proteins and abrogates BCR signaling to result in malignant cell death. (**A**) Crystal structures of NX-2127 hook bound to WT (yellow, PDB ID 8GC7) and L528W mutant (blue, PDB ID 8GC8) BTK proteins aligned on their C-lobes. View into the BTK active site with the proteins shown as ribbons. The ligands and resistance mutation sites are shown as sticks and highlighted in light red for the WT and in purple for the L528W mutant structure. P-loop residues have been removed for visibility. (**B**) NX-2127 hook (pink) bound BTK L528W mutant shown as gray ribbons with highlighted C-spine (blue mesh and sticks) and R-spine (yellow mesh and sticks). Three mutation sites covered in this study are located in the C-spine and are indicated as magenta sticks. The R-spine is not fully assembled with M449 on the αC-helix not placed in the correct position. For reference, a WT BTK structure in active C-helix "in" conformation (PDB ID 3K54) is depicted in cyan ribbons, where the K430 and E445 side chains (shown as sticks) form the required salt bridge. Cβ atoms of the salt bridge residues from K430 and E445 are shown as green spheres for comparison with the same atoms in the L528W structure shown as red spheres. This salt bridge between K430 and E445 side chains was not observed in the L528W structure. (**C**) Dose curves of knock-in TMD8 cells expressing WT and mutant (C481S, V416L, T474I, and L528W) BTK treated with NX-2127 for 24 hours and 50% degradation concentration (DC_{50})

for BTK, IKZF1 (Ikaros), and IKZF3 (Aiolos) were determined. (**D**) Measurements of intracellular calcium (Ca^{2+}) release upon IgM-mediated cross-linking of the BCR over time in knock-in TMD8 cells after 24-hour treatment with either vehicle (top panel) or 1 μM NX-2127 (bottom panel). (**E**) Heatmap of 50% growth inhibition (GI_{50}) of TMD8 cells expressing WT and mutant BTK after 72-hour treatment with NX-2127, BTK inhibitors, and immunomodulatory drugs. Data in (C) and (E) were averaged from n = 3 independent experiments, and mean ± SEM is displayed.

displacement of the N-lobe in the L528W mutant kinase transitions the C-helix close to the C-helix "in" conformation but does not allow the formation of the K430-to-E445 salt bridge (Cβ-Cβ distance >10 Å) (*49*) (Fig. 4B). Because the distinctive C-helix conformation shifts the position of M449, the regulatory (R)–spine in the L528W mutant structure cannot be fully assembled (fig. S4C) (*31*, *50*). The superposition of an adenosine diphosphate (ADP)–bound c-Src structure [Protein Data Bank (PDB) ID 5XP7] reveals a 1.5-Å clash between the mutant tryptophan and the ADP ribose, suggesting that binding of ATP will result in a similar N-lobe movement as observed in the ligand-bound L528W mutant structure (fig. S4D). As determined in the FRET-based activity assay, the K_m of ATP only decreases about twofold from WT to the L528W mutant, but the overall catalytic efficiency (k_{cat}/K_m) decreases >100-fold (Fig. 1C). We hypothesize that even though ATP binding is still allowed in the L528W mutant, steric hindrance posed by the tryptophan residue reduces the conformational flexibility that is necessary for catalysis (*51*).

NX-2127 degrades recurrent drug-resistant forms of mutant BTK and inhibits BCR signaling

As described earlier, we used CRISPR-Cas9 editing to introduce key BTK mutations into TMD8 cells to ensure that mutant BTK was expressed from the endogenous promoter at physiological levels and turnover rates (fig. S1C). Superphysiological overexpression of BTK drastically alters cellular sensitivity to BTK-targeted agents (fig. S5). Conversely, weak overexpression of mutant BTK is confounded by coexpression of WT BTK, which may alter signaling biology and assessments of antimutant activity. We used CRISPR knock-in lines to quantify degradation of WT and mutant BTK protein by determining the concentration of NX-2127 that degrades 50% of BTK protein (DC_{50}) in knock-in TMD8 cells expressing WT and mutant (C481S, V416L, T474I, and L528W) BTK. After 24 hours of treatment, NX-2127 achieved dose-dependent BTK degradation with calculated DC_{50} values in the BTK WT (1.9 nM) and mutant C481S (9.7 nM), V416L (4.2 nM), T474I (2.4 nM), and L528W (1.9 nM) lines. Additionally, NX-2127 promoted degradation of IKZF1 and IKZF3 in BTK WT and mutant lines with calculated DC_{50} values for IKZF1 (45.0 to 82.5 nM) and IKZF3 (18.3 to 31.2 nM) (Fig. 4C). To assess the effects of NX-2127 treatment on downstream signaling in knock-in TMD8 cell lines, we repeated the Ca^{2+} flux assay both in the presence and absence of NX-2127. Our results show consistent IgM-induced hyperactive Ca^{2+} flux in all BTK mutants regardless of expression level or enzymatic class. Notably, after 24-hour treatment with NX-2127, downstream Ca^{2+} signaling was completely abrogated in all BTK-expressing TMD8 cells (Fig. 4D). Effective inhibition of BCR signaling is known to decrease surface CD86 and HLA-DR expression while also increasing surface IgM on malignant B cells. To quantitatively compare the responsiveness of BTK mutants to currently available treatments, we analyzed suppression of surface CD86, HLA-DR (human leukocyte antigen–DR isotype), and upregulation of surface IgM by calculating the half maximal effective concentration (EC_{50}) of surface marker expression after 24-hour treatment with each compound. As expected, the C481S mutation prevented biomarker modulation by all covalent BTK inhibitors but was sensitive to noncovalent BTK inhibition. NX-2127 retained the ability to modulate surface marker expression in BTK WT and all mutant TMD8 cells, showing decreased CD86 and HLA-DR and increased IgM (fig. S6, A to C).

Considering the diminished enzymatic activity in BTK mutants V416L and L528W, the ability of NX-2127 to block downstream BCR signaling in these cells by degrading BTK further supports the novel noncatalytic scaffold function of BTK. We also assessed the selectivity of NX-2127 within the Tec family of kinases, and NX-2127 demonstrated >100-fold selectivity for BTK over Tec, ITK, and RLK (fig. S6, D and E). NX-2127 also displayed high proteome-wide selectivity, with only one non-BTK protein [heme-binding protein 1 (HEBP1)] significantly decreased in TMD8 cells after NX-2127 treatment (fig. S6F). We were not able to verify HEBP1 as down-regulated upon NX-2127 treatment using an orthogonal method owing to unavailability of HEBP1-specific antibodies.

Finally, to assess the impact of NX-2127 treatment on malignant B cell survival, we quantified viability of WT and BTK mutant cells treated with NX-2127, BTK inhibitors, and immunomodulatory drugs. As expected, the C481S mutation abrogated the antiproliferative activity of covalent BTK inhibitors, and the V416L, T474I, and L528W mutations eliminated the antiproliferative activity of pirtobrutinib (Fig. 4E). Consistent with the reduction in biomarker modulation, the L528W mutation reduced or eliminated the antiproliferative activity of ibrutinib and zanubrutinib, and the V416L and T474I mutations reduced the activity of acalabrutinib. By contrast, NX-2127 displayed potent antiproliferative activity in all lines, regardless of mutation. This impact of NX-2127 is due to its ability to degrade mutant BTK, as the immunomodulatory drugs pomalidomide and lenalidomide had significantly lower antiproliferative activity in TMD8 cells at similar concentrations (fig. S7).

Clinical benefit of NX-2127 and achievement of BTK degradation in relapsed/refractory CLL patients

Given the above preclinical data, we initiated a first-in-human phase 1 clinical trial of NX-2127 in relapsed/refractory B cell malignancies, including CLL (NCT04830137). In this ongoing open-label, dose-escalation phase 1 clinical trial, patients were treated with the oral BTK degrader NX-2127. At the time of data cutoff for this nonprespecified interim analysis (21 September 2022), 23 CLL/SLL (small lymphocytic lymphoma) patients were enrolled at dose levels of 100, 200, and 300 mg. Available baseline blood specimens from 21 CLL patients were assessed for BTK mutational status before treatment with NX-2127. Sequencing analysis revealed that 11/21 patients had no detectable BTK mutations, 5/21 patients harbored kinase-impaired mutations (L528W, C481R, and/or V416L), and 5/21 patients displayed kinase-proficient mutations (C481S, T474F, and/or T474I). No additional mutations were found in the B cell receptor signaling pathway in the samples tested. Other common gene mutations in CLL patients such as *TP53*, *ATM*, *SF3B1*, *SPEN*, and *NOTCH1* were detected in these patients (fig. S8). Use of serial intracellular flow cytometric analysis for BTK allowed us to assess the kinetics of BTK degradation in peripheral blood of patients treated with NX-2127 (Fig. 5A). BTK degradation was quantified using BTK mean fluorescence intensity (MFI) measurement in B cells ($CD19^+CD3^-$). NX-2127 exposure resulted in BTK degradation in circulating B cells as measured by decreasing BTK MFI values with maximal degradation observed as early as day 8 of the first cycle. The rate and degree of degradation were similar in all patients regardless of their mutational status. In addition, similarly sustained BTK degradation was also observed in all WT and BTK resistance mutations throughout the daily dosing interval through the first 28-day cycle. For patients with BTK mutations, degradation of BTK was independent of mutation type and level of enzymatic activity. These results suggest that NX-2127 can degrade BTK in relapsed/refractory CLL patients, including those patients who have acquired BTK resistance

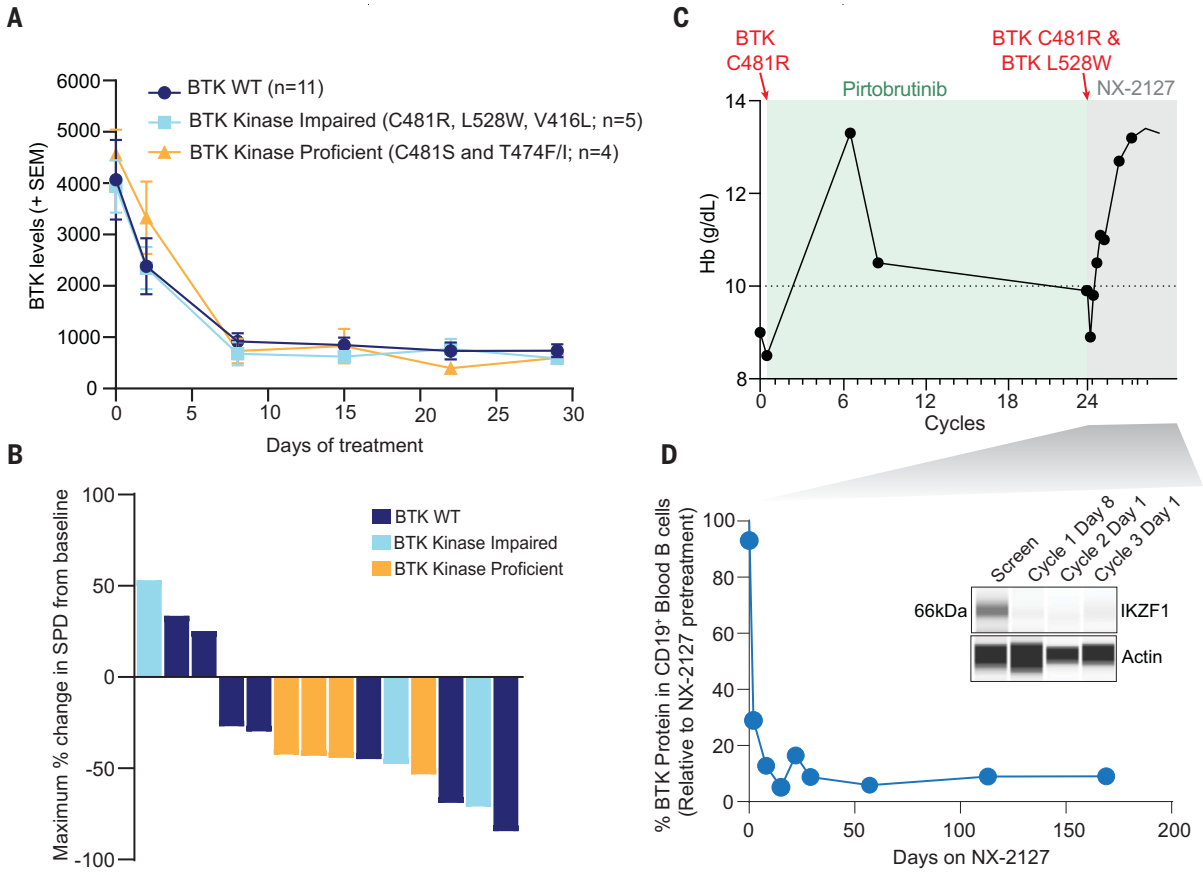

Fig. 5. Effective BTK and IKZF1 degradation and clinical response in CLL patients treated with NX-2127. At the time of the datacut (September 2022), 21 patients were sequenced by next-generation sequencing, 20 patients were evaluated for BTK degradation, and 14 patients were disease evaluable. (**A**) Intracellular BTK levels in $CD19^+$ $CD3^-$ cells from the peripheral blood of CLL patients with distinct categories of BTK mutations treated with NX-2127. Mean ± SEM values for each time point are shown. (**B**) Maximum percent change in sum of the product of the diameters (SPD) of tumors from baseline in patients from (A). (**C**) Hemoglobin values in a representative CLL BTK C481R mutant patient at the start of treatment with pirtobrutinib followed by transition to NX-2127 after development of resistance to pirtobrutinib due to acquisition of a new BTK L528W mutation. (**D**) Percent of BTK protein in $CD19^+$ cells in the peripheral blood as well as IKZF1 protein levels in peripheral blood mononuclear cells (inset) after start of NX-2127 treatment of patient from (C).

mutations as a result of prior covalent and/or noncovalent BTK inhibitor therapies.

Furthermore, in addition to BTK degradation observed in the peripheral blood, we have observed clinical activity of NX-2127 in CLL patients. For example, in 11 of 14 evaluable CLL patients, we observed an improvement in the sum of the product of the diameters (SPD) of the target lesions in a broad group of patients harboring both kinase-proficient and kinase-impaired BTK resistance mutations, as well as various other known recurrent CLL mutations (Fig. 5B and fig. S8). NX-2127 was safe and well tolerated in this patient population (table S2). One exemplary male patient with CLL with BTK C481R mutation who had progressed on multiple prior therapies, including ibrutinib and venetoclax, was subsequently treated with pirtobrutinib and developed a BTK L528W mutation. He was then treated with NX-2127 with a hematologic improvement, resolution of his anemia, and improvement in splenomegaly, with a best response of partial response by International Workshop on CLL (iwCLL) criteria (*52*). Treatment with NX-2127 resulted in >90% BTK and substantial IKZF1 degradation in $CD19^+$ B cells (Fig. 5, C and D).

Discussion

The dependency of CLL and other B cell lymphomas on BTK enzymatic activity has led to the clinical success of several generations of BTK enzymatic inhibitors. However, the clinical activity of existing BTK inhibitors is eventually limited by acquisition of on-target resistance mutations, several of which cause resistance across classes of covalent and noncovalent BTK inhibitors. Identification of novel targeted agents that can broadly target different classes of BTK inhibitor resistance mutations is critical to provide subsequent treatment options for patients.

In this study, we identified that BTK inhibitor resistance mutations fall into two distinct functional categories: those that preserve kinase activity and those with impaired kinase function based on their in vitro and in cellular enzymatic activities. Despite a lack of BTK autophosphorylation in cells with impaired kinase function, downstream readouts of BCR signaling such as calcium release, ERK (extracellular signal–regulated kinase) phosphorylation, and cell survival were maintained, suggesting that other kinases may compensate for the absence of BTK enzymatic activity. Evidence for this hypothesis was seen in phosphoproteomics in which BTK L528W cells showed diminished phosphorylation of BTK but increases in the activity of several kinases that were distinct compared with BTK WT or kinase-proficient mutations. Ultimately, we found that mutations that diminish BTK kinase activity simultaneously alter the conformation of BTK in a manner that induces interactions with surrogate kinases that propagate downstream BCR signaling. This scaffold neofunction of BTK led to our hypothesis that inducing BTK degradation might simultaneously eliminate the scaffold effect of BTK mutants with impaired kinase function as well as the enzymatic

activity of those BTK mutants that retain kinase function. Indeed, we demonstrate that malignant cells remain dependent on this novel scaffold function of inhibitor-resistant BTK, as preclinical and clinical BTK degradation resulted in antitumor activity.

As part of this study, we newly identified three BTK inhibitor–resistant mutants with impaired kinase activity (M437R, V416L, and L528W). Recent work by Dhami *et al.* demonstrated that rare C481 substitutions (including C481F, C481Y, and C481R) also impair BTK's kinase activity and similarly mediate resistance to covalent BTK inhibitors (*28*). While kinase-impaired C481 variants are rare among reports of BTK mutations causing resistance to BTK inhibitors, we and others have observed increased incidence of BTK V416L and L528W mutations in resistance to the noncovalent BTK inhibitor pirtobrutinib (*5*) and the covalent inhibitor zanubrutinib (*9*). Our data therefore have important implications for the therapeutic sequencing of targeted BTK agents and application of zanubrutinib and pirtobrutinib (as well as other BTK inhibitors), as they are now FDA-approved and are beginning to be used more broadly in clinical practice.

Differences between the level of enzymatic activity of inhibitor-resistant BTK mutations and the previously reported effects of BTK knockout or loss-of-function mutations led to the hypothesis that these kinase-impaired mutant isoforms of BTK could be acting as scaffolds for other kinases to bind and activate signaling. Indeed, IP experiments followed by mass spectrometry revealed several signaling proteins uniquely interacting with BTK L528W. Orthogonal validation by gel electrophoresis and mass spectrometry or immunoblot revealed distinctive interactions between this mutant form of BTK and the signaling proteins HCK and ILK.

The discovery of enzymatically impaired mutations within BTK that engender gain-of-function activity follows a similar paradigm to mutations in the serine/threonine kinase BRAF. Although kinase-active mutations in BRAF (such as BRAF V600E) are common in many cancers, the most common class of BRAF mutations in non–small cell lung cancer have either low enzymatic activity or are kinase dead (*53*, *54*). Interestingly, kinase-impairing mutations in BRAF still result in activation of the MAP kinase pathway as they promote binding of BRAF/CRAF complexes to RAS and ultimately enhance RAS pathway activation (*53*). Thus, kinase-inactivating BTK mutations analogously enhance BCR signaling through interactions with surrogate kinases. Another study found that rapid resistance to BTK inhibition can occur through nongenetic changes that enable the guanosine triphosphatase RAC2 to substitute for BTK in the activation of phospholipase Cγ2 (PLCγ2) (*55*).

Targeted protein degradation is a novel therapeutic targeting mechanism that overcomes some challenges associated with traditional small molecule–based inhibition. Development of such degraders requires an intimate knowledge of the target, linker technology, and understanding of E3 ubiquitin ligase recruitment strategies. NX-2127 is a first-in-class heterobifunctional BTK degrader that consists of a BTK-binding hook linked to a cereblon recruitment harness that potently and selectively targets BTK, IKZF1, and IKZF3 for proteasomal degradation. Thus, NX-2127 degrades IKZF1/3 in addition to BTK through defined molecular interactions, an important mechanistic property of the drug. Using the hook of NX-2127, we show by FRET and SPR assays that NX-2127 is able to bind to all mutant forms of BTK studied, whereas other covalent and noncovalent BTK inhibitors tested do not. Furthermore, in NanoBRET assays, NX-2127 induced dose-dependent ternary complex formation between cereblon and BTK WT or mutant forms in cells. Cooperativity assays showed that this stable complex formation led to cooperativity indices of >1, consistent with greater BTK binding by NX-2127 in the presence of cereblon.

Importantly, NX-2127 degraded BTK WT and all classes of BTK inhibitor resistance mutations at nanomolar concentrations. NX-2127's ability to bind BTK mutants with impaired kinase function was shown by solving the crystal structure of NX-2127 bound to the kinase domain of BTK L528W. Consistent with our hypothesis that degrading mutant BTK would abrogate this previously unappreciated scaffold function, we observed a block in calcium release and sustained cell killing after treatment with NX-2127 in BTK V416L and L528W cells, similar to that observed for cells harboring enzymatically active BTK mutants or BTK WT. Our results show that the catalytic nature of degraders, coupled with their reduced reliance on binary target binding, provides more resilience in the context of mutational resistance when compared with inhibitors that depend on prolonged target occupancy.

Given these encouraging results, a first-in-human trial of NX-2127 was initiated for patients with relapsed/refractory B cell malignancies, including CLL (NCT04830137). One notable patient with CLL who had progression of disease on pirtobrutinib and acquired a kinase-impaired BTK L528W mutation was treated with NX-2127 and has had a clinical response associated with degradation of BTK in the peripheral blood during ongoing treatment on NX-2127. In additional patients with relapsed/refractory CLL, and known BTK mutational status, on-target BTK degradation and clinical responses were seen independent of BTK mutation status (WT, kinase proficient, or kinase impaired). The clinical trial is ongoing in patients with CLL and other B cell malignancies. These results provide the first evidence in humans that BTK degradation is achievable by NX-2127 and may be associated with clinical responses even in patients with previously described and newly discovered BTK inhibitor–resistant forms of BTK mutations.

Materials and methods summary

Clinical study design

NCT04830137 is a first-in-human phase 1a/1b multicenter, US-based, open-label, phase 1 dose-escalation (phase 1a) and cohort-expansion (phase 1b) trial, evaluating the safety, tolerability, and preliminary efficacy of NX-2127 in adult patients with relapsed/refractory CLL and B cell malignancies who have received at least two prior systemic therapies [or at least one prior therapy for patients with Waldenstrom macroglobulinemia (WM) or primary central nervous system lymphoma (PCNSL)] and for whom no other therapies are known to provide clinical benefit. Phase 1b will investigate the efficacy of NX-2127 and the dose selected in phase 1a in up to five cohorts of patients with relapsed/refractory B cell malignancy indications who have received at least two prior systemic therapies (or at least one prior therapy for patients with WM or PCNSL). These cohorts will include patients with CLL or SLL with or without BTK C481 mutations, MCL, follicular lymphoma, marginal zone lymphoma, PCNSL, DLBCL, and WM.

Primary outcome measures include the number of participants with protocol-specified dose-limiting toxicities, to establish the maximum tolerated dose and/or recommended phase 1b dose (RP1bD) of NX-2127, evaluate the clinical activity at the RP1bD by overall response rate (ORR) as assessed by the investigator, as well as the number of participants with adverse events. Secondary outcome measures include characterizing the pharmacokinetic profile of NX-2127, the duration of response, progression-free survival, complete response rate, and overall survival as assessed by the investigator, as well as further evaluating the safety and tolerability of NX-2127.

Eligible subjects were ≥18 years old and had measurable disease per disease-specific response criteria, an Eastern Cooperative Oncology Group score of ≤1, and adequate bone marrow function. Exclusion criteria were preestablished and included history of CNS lymphoma/leukemia in remission for <2 years (non-PCNSL indications) or evidence of disease outside of the CNS (PCNSL patients); history of autoimmune disease; infection with HIV (with the exception of well-controlled HIV); active viral reactivation; clinically significant, uncontrolled cardiac, cardiovascular disease, or history of myocardial infarction within 6 months of planned start of study drug; or administration of any strong CYP3A inducer or inhibitor for 14 days before the first

dose of study drug, and any P-glycoprotein inhibitors or moderate inducers of CYP3A for 7 days. For the purpose of this report, we focused only on the population of patients with CLL.

Given the exploratory nature of the phase 1a/b study design, the sample size is not based on power calculations and is determined by practical, rather than power, considerations. With approximately 20 evaluable patients (i.e., meeting efficacy evaluable criteria) anticipated, the precision of the point estimate for the ORR, based on the width of its 95% ClopperPearson confidence interval (CI), ranges from a width of 0.247 (95% CI = [0.001, 0.249]) for a response rate of 1/20 to a maximum width of 0.456 (95% CI = [0.272, 0.728]) when the response rate is 10/20.

Patients

The CLL patients and samples analyzed included in the present manuscript were from a nonprespecified interim analysis. Although age, sex and gender, and ethnicity were collected for all study participants, because of the small numbers, we are not reporting these because of privacy concerns. Patients received NX-2127 orally once daily in 28-day cycles starting at 100 mg. Peripheral blood specimens were obtained from patients to define BTK mutational status and BTK levels before NX-2127 treatment. Additional blood specimens were also obtained longitudinally to monitor and determine BTK degradation. All patients provided written informed consent, and the study protocol was approved by each institutional review board.

Mutational analysis was performed with blood specimens obtained at baseline using a targeted next-generation sequencing (NGS) Lymphoid 133 NGS panel (NeoGenomics, Fort Myers, FL) comprising 133 commonly mutated genes found in hematologic malignancies using DNA isolated from the peripheral blood. *BTK* mutations with variant allele frequencies of ≥5% were included in the analysis. On the basis of this analysis, we classified patients with no detectable BTK mutation as WT; patients with either C481R, L528W, or V416L as BTK kinase–impaired mutants; and those who harbored C481S, T474F, or T474I as BTK kinase–proficient mutants. Some patients harbored both kinase-impaired and kinase-proficient BTK mutations. In such cases, we assigned patients as BTK kinase–impaired regardless of co-occurrence of kinase-proficient mutation.

BTK degradation was assessed longitudinally in the peripheral blood using a validated fit-for-purpose flow cytometry assay (Precision for Medicine, Inc., Bethesda, MD) designed to quantify BTK degradation in circulating B cells ($CD19^+CD3^-$); B cells were gated on $CD45^+$ $CD14^-$ lymphocytes. BTK geometric MFI was quantified in B cells, and BTK MFI was reported after background subtraction.

Western blot

Whole-cell lysates were prepared with Pierce IP lysis buffer (89900) supplemented with protease and phosphatase inhibitors (78446) (Thermo Scientific, Waltham, MA). Protein concentration was determined using Pierce BCA Protein Assay kit (23227) (Thermo Scientific, Waltham, MA). Thirty micrograms of total protein was separated by electrophoresis on a 4–20% mini-PROTEAN TGX gels (4561094), transferred onto a PVDF membrane, and probed with antibodies against phospho-BTK (Tyr223) (87457S), phospho-AKT (Ser473) (4060S), phospho-Erk (Thr202/Tyr204) (4370S), phospho-PLCγ2 (Tyr1217) (3871S), total BTK (8547S), PLCγ2 (5512S), AKT (4691S), ERK1/2 (4695S), HCK (14643S) from (Cell Signaling Technologies Danvers, MA), ILK1 (A0901) (Abclonal Woburn, MA), and Anti-Flag (F3165) (Sigma, Burlington, MA). βactin HRP (8H10D10) was used at 1:2000. Membranes were visualized by ECL detection reagent (170-5061) (Bio-Rad Hercules, CA) following the manufacturer's protocol.

Calcium flux

Intracellular calcium levels in knock-in BTK WT, C481S, V416L, T474I, or L528W TMD8 cells were either treated with vehicle [dimethyl sulfoxide (DMSO)] or 1 μM of NX-2127 for 24 hours before staining using Indo-1 (1223) (Life Technologies) on an LSR-Fortessa-HTS flow cytometer. Indo-1 Violet and Indo-1 Blue levels were measured for two minutes immediately followed by stimulation with 10 μg/ml of anti-human IgM (2020-01) (Southern Biotech) and then measured continuously for 10 min. BTK WT or L528W mutant cells expressing shHCK or shILK were treated with doxycycline for 48 hours before being stained using Indo-1 and measured as described above.

Phosphoproteomics

TMD8 cells expressing BTK WT, T474I, or L528W were treated with either vehicle (DMSO) or 1 μM of pirtobrutinib for 1 hour in triplicate. Cells were then all stimulated with 10 μg/ml of anti-human IgM (2020-01) (Southern Biotech) for 15 min and treated with pervanadate solution (0.25 mM sodium orthovanadate, 0.3% hydrogen peroxide, and phosphate-buffered saline) for 10 min for phosphotyrosine enrichment. Cells were collected, pelleted, and lysed in MS lysis buffer (0.5% Nonidet-40, 150 nM NaCl, 10 mM KCl, 1.5 mM $MgCl_2$, 10 mM Tris-HCl, pH = 8) supplemented with 10 μg/ml of protease and phosphatase inhibitors. Lysates were cleared by centrifugation at 21,000*g* for 30 min at 4°C, and protein concentration was measured by bicinchoninic acid assay. One milligram of nuclear extracts was denatured in 2% SDS/2% SDC/200 mM EPPS at 60°C for 15 min followed by sonication. Samples were reduced with 5 mM tris(2-carboxyethyl)phosphine, alkylated with 10 mM iodoacetamide, and quenched with 10 mM dithiothreitol. Protein was chloroform–methanol precipitated. Protein was reconstituted in 200 mM EPPS (pH 8.5) and digested by Lys-C overnight and trypsin for 6 hours, both at a 1:50 protease-to-peptide ratio. Digested peptides were quantified using a Nanodrop at 280 nm, and 500 μg of the peptide from each sample was labeled with 500 μg tandem mass tag (TMT) reagent using a 16-plex TMT kit (*56*). TMT labels were checked; 100 ng of each sample was pooled, desalted, and analyzed by short SPS-MS3 (synchronous precursor selection mass spectrometry to the third) method; and, using normalization factor, samples were bulk mixed at 1:1 across all channels and desalted using a 500 mg Sep-Pak solid-phase extraction column and dried using vacuum centrifugation.

Tyrosine phosphorylated peptides enrichment

Desalted dried isobaric labeled peptides (4 mg) were resuspended in 1.4 ml of ice-cold high specificity and sensitivity immunoaffinity purification (HS IAP) bind buffer [50 mM MOPS (pH 7.2), 10 mM sodium phosphate, and 50 mM NaCl] and centrifuged at maximum speed for 5 min at 4°C to remove any insoluble material. Supernatants (pH ~7.5) were incubated with the washed PTMScan Phospho-Tyrosine Motif (Y*) (P-Tyr-1000) (Cell Signaling Technology) immunoaffinity magnetic beads for 2 hours at 4°C with gentle end-over-end rotation. After centrifugation at 2000*g* for 1 min, beads were washed four times with ice-cold HS IAP wash buffer and three times with ice-cold HPLC water. The phosphotyrosine peptides were eluted twice with 0.15% trifluoroacetic acid, desalted using SDB-RPS StageTip, and dried by vacuum centrifugation.

Liquid chromatography with tandem mass spectrometry analysis and data processing

The isobaric labeled dried phosphotyrosine peptides were dissolved in 10 μl of (3% acetonitrile/0.1% formic acid) and analyzed on an Orbitrap Fusion mass spectrometer coupled to a Dionex Ultimate 3000 (Thermo Fisher Scientific) using the MSA-SPS-MS3 and NL SPS-MS3 method (*57*). Peptides were separated on an EASY-Spray C18 25cm column (Thermo Scientific). Peptide elution and separation were achieved at a nonlinear flow rate of 250 nl/min using a gradient of 5% to 30% of buffer B [0.1% (v/v) formic acid, 100% acetonitrile] for 120 min with a temperature of the column maintained at 40°C during the entire experiment. For both methods, MS1 data were collected using the Orbitrap (120,000 resolution; maximum injection time: 50 ms; AGC 4×10^5). Determined charge states between 2 and 4 were required for sequencing, and a 60-s dynamic exclusion window was used. Data-dependent top10 MS2 scans were performed in the ion trap with collision-induced dissociation (CID) fragmentation (Turbo; NCE

30%; maximum injection time 54 ms; AGC 5×10^4). MS3 quantification scans were performed using the multi-notch MS3-based TMT method (10 SPS ions; 50,000 resolution; NCE 55% for MSA-SPS-TMT and 35% for NL-SPS-TMT maximum injection time 100 ms; AGC 1×10^5) using the Orbitrap.

Phosphoproteomics mass spectrometry data bioinformatics

Raw mass spectrometric data were analyzed using Proteome Discoverer 2.4 to perform database search and TMT reporter ions quantification. TMT tags on lysine residues and peptide N termini (+304.2071 Da) and the carbamidomethylation of cysteine residues (+57.021 Da) were set as static modifications, while the oxidation of methionine residues (+15.995 Da), deamidation (+0.984) on asparagine and glutamine, and phosphorylation (+79.966) on serine, threonine, and tyrosine were set as a variable modification. Data were searched against a UniProt Human database with peptide-spectrum match (PSMs) and protein-level false discovery rate (FDR) at 1% FDR. The signal-to-noise (S/N) measurements of each protein normalized so that the sum of the signal for all proteins in each channel was equivalent to account for equal protein loading. Phosphopeptide identification and quantification were imported into Perseus (Version 1.2.2) to filter and annotate data. Filtered data were then processed in R studio (Version 4.1.3) using the Bioconductor software package *limma* (*58*), to test for statistical analysis (FDR<0.05). Adjusted *P* values were negatively logarithmized ($-\log_{10}$) and fold-change (FC) values (mutant/WT) were logarithmized ($\log_2$) to identify proteins demonstrating statistically significant changes in abundance. Data was visualized as volcano plots using R package *ggplot2* (*59*) with significance cutoffs for FC and *P* value of −1,1 and −1.3,1.3, respectively. KSEA was performed using the R package *KSEAapp* to show estimated changes in kinase activity based on phosphorylation changes of identified substrates.

REFERENCES AND NOTES

1. R. E. Davis *et al*., Chronic active B-cell-receptor signalling in diffuse large B-cell lymphoma. *Nature* **463**, 88–92 (2010). doi: 10.1038/nature08638; pmid: 20054396
2. R. W. Hendriks, S. Yuvaraj, L. P. Kil, Targeting Bruton's tyrosine kinase in B cell malignancies. *Nat. Rev. Cancer* **14**, 219–232 (2014). doi: 10.1038/nrc3702; pmid: 24658273
3. D. A. Bond, J. A. Woyach, Targeting BTK in CLL: Beyond ibrutinib. *Curr. Hematol. Malig. Rep.* **14**, 197–205 (2019). doi: 10.1007/s11899-019-00512-0; pmid: 31028669
4. J. A. Burger *et al*., Ibrutinib as initial therapy for patients with chronic lymphocytic leukemia. *N. Engl. J. Med.* **373**, 2425–2437 (2015). doi: 10.1056/NEJMoa1509388; pmid: 26639149
5. E. Wang *et al*., Mechanisms of resistance to noncovalent Bruton's tyrosine kinase inhibitors. *N. Engl. J. Med.* **386**, 735–743 (2022). doi: 10.1056/NEJMoa2114110; pmid: 35196427
6. R. W. Hendriks, Drug discovery: New Btk inhibitor holds promise. *Nat. Chem. Biol.* **7**, 4–5 (2011). doi: 10.1038/nchembio.502; pmid: 21164510
7. Y. Song *et al*., Treatment of patients with relapsed or refractory mantle-cell lymphoma with zanubrutinib, a selective inhibitor of Bruton's tyrosine kinase. *Clin. Cancer Res.* **26**, 4216–4224 (2020). doi: 10.1158/1078-0432.CCR-19-3703; pmid: 32461234
8. F. Cameron, M. Sanford, Ibrutinib: First global approval. *Drugs* **74**, 263–271 (2014). doi: 10.1007/s40265-014-0178-8; pmid: 24464309
9. J. R. Brown *et al*., Zanubrutinib or ibrutinib in relapsed or refractory chronic lymphocytic leukemia. *N. Engl. J. Med.* **388**, 319–332 (2023). doi: 10.1056/NEJMoa2211582; pmid: 36511784
10. J. Muñoz, J. Paludo, S. Sarosiek, J. J. Castillo, Coming of age for BTK inhibitor therapy: A review of zanubrutinib in Waldenström macroglobulinemia. *Cells* **11**, 3287 (2022). doi: 10.3390/cells11203287; pmid: 36291152
11. H. Y. Estupiñán *et al*., BTK gatekeeper residue variation combined with cysteine 481 substitution causes super-resistance to irreversible inhibitors acalabrutinib, ibrutinib and zanubrutinib. *Leukemia* **35**, 1317–1329 (2021). doi: 10.1038/s41375-021-01123-6; pmid: 33526860
12. J. A. Burger *et al*., Clonal evolution in patients with chronic lymphocytic leukaemia developing resistance to BTK inhibition. *Nat. Commun.* **7**, 11589 (2016). doi: 10.1038/ncomms11589; pmid: 27199251
13. R. R. Furman *et al*., Ibrutinib resistance in chronic lymphocytic leukemia. *N. Engl. J. Med.* **370**, 2352–2354 (2014). doi: 10.1056/NEJMc1402716; pmid: 24869597
14. J. A. Woyach *et al*., Resistance mechanisms for the Bruton's tyrosine kinase inhibitor ibrutinib. *N. Engl. J. Med.* **370**, 2286–2294 (2014). doi: 10.1056/NEJMoa1400029; pmid: 24869598
15. S. D. Reiff *et al*., The BTK inhibitor ARQ 531 targets ibrutinib-resistant CLL and Richter transformation. *Cancer Discov.* **8**, 1300–1315 (2018). doi: 10.1158/2159-8290.CD-17-1409; pmid: 30093506
16. D. Gu, H. Tang, J. Wu, J. Li, Y. Miao, Targeting Bruton tyrosine kinase using non-covalent inhibitors in B cell malignancies. *J. Hematol. Oncol.* **14**, 40 (2021). doi: 10.1186/s13045-021-01049-7; pmid: 33676527
17. J. A. Woyach *et al*., *Cancer Discov.* **14**, 66–75 (2024).
18. J. L. Jensen, A. R. Mato, C. Pena, L. E. Roeker, C. C. Coombs, The potential of pirtobrutinib in multiple B-cell malignancies. *Ther. Adv. Hematol.* **13**, 1–10 (2022). doi: 10.1177/20406207221101697; pmid: 35747462
19. P. Blombery *et al*., Enrichment of BTK Leu528Trp mutations in patients with CLL on zanubrutinib: Potential for pirtobrutinib cross-resistance. *Blood Adv.* **6**, 5589–5592 (2022). doi: 10.1182/bloodadvances.2022008325; pmid: 35901282
20. S. M. Handunnetti *et al*., BTK Leu528Trp - a potential secondary resistance mechanism specific for patients with chronic lymphocytic leukemia treated with the next generation BTK inhibitor zanubrutinib. *Blood* **134** (suppl. 1), 170 (2019). doi: 10.1182/blood-2019-125488
21. A. Naeem *et al*., Pirtobrutinib targets BTK C481S in ibrutinib-resistant CLL but second-site BTK mutations lead to resistance. *Blood Adv.* **7**, 1929–1943 (2023). doi: 10.1182/bloodadvances.2022008447; pmid: 36287227
22. L. Sedlarikova, A. Petrackova, T. Papajik, P. Turcsanyi, E. Kriegova, Resistance-associated mutations in chronic lymphocytic leukemia patients treated with novel agents. *Front. Oncol.* **10**, 894 (2020). doi: 10.3389/fonc.2020.00894; pmid: 32670873
23. A. J. Mohamed, B. F. Nore, B. Christensson, C. I. Smith, Signalling of Bruton's tyrosine kinase, Btk. *Scand. J. Immunol.* **49**, 113–118 (1999). doi: 10.1046/j.1365-3083.1999.00504.x; pmid: 10075013
24. H. Suzuki *et al*., PI3K and Btk differentially regulate B cell antigen receptor-mediated signal transduction. *Nat. Immunol.* **4**, 280–286 (2003). doi: 10.1038/ni890; pmid: 12563258
25. S. Middendorp, G. M. Dingjan, A. Maas, K. Dahlenborg, R. W. Hendriks, Function of Bruton's tyrosine kinase during B cell development is partially independent of its catalytic activity. *J. Immunol.* **171**, 5988–5996 (2003). doi: 10.4049/jimmunol.171.11.5988; pmid: 14634110
26. A. D. Buhimschi *et al*., Targeting the C481S ibrutinib-resistance mutation in Bruton's tyrosine kinase using PROTAC-mediated degradation. *Biochemistry* **57**, 3564–3575 (2018). doi: 10.1021/acs.biochem.8b00391; pmid: 29851337
27. D. Dobrovolsky *et al*., Bruton tyrosine kinase degradation as a therapeutic strategy for cancer. *Blood* **133**, 952–961 (2019). doi: 10.1182/blood-2018-07-862953; pmid: 30545835
28. D. Zhang *et al*., NRX-0492 degrades wild-type and C481 mutant BTK and demonstrates in vivo activity in CLL patient-derived xenografts. *Blood* **141**, 1584–1596 (2023). doi: 10.1182/blood.2022016934; pmid: 36375120
29. K. Dhami *et al*., Kinase-deficient BTK mutants confer ibrutinib resistance through activation of the kinase HCK. *Sci. Signal.* **15**, eabg5216 (2022). doi: 10.1126/scisignal.abg5216; pmid: 35639855
30. H. Yuan *et al*., BTK kinase activity is dispensable for the survival of diffuse large B-cell lymphoma. *J. Biol. Chem.* **298**, 102555 (2022). doi: 10.1016/j.jbc.2022.102555; pmid: 36183831
31. J. A. Burger, Treatment of chronic lymphocytic leukemia. *N. Engl. J. Med.* **383**, 460–473 (2020). doi: 10.1056/NEJMra1908213; pmid: 32726532
32. A. J. Linley *et al*., Kinobead profiling reveals reprogramming of BCR signaling in response to therapy within primary CLL cells. *Clin. Cancer Res.* **27**, 5647–5659 (2021). doi: 10.1158/1078-0432.CCR-21-0161; pmid: 34380642
33. L. Zhang *et al*., Characterization of the novel broad-spectrum kinase inhibitor CTx-0294885 as an affinity reagent for mass spectrometry-based kinome profiling. *J. Proteome Res.* **12**, 3104–3116 (2013). doi: 10.1021/pr3008495; pmid: 23692254
34. A. R. Poh, R. J. O'Donoghue, M. Ernst, Hematopoietic cell kinase (HCK) as a therapeutic target in immune and cancer cells. *Oncotarget* **6**, 15752–15771 (2015). doi: 10.18632/oncotarget.4199; pmid: 26087188
35. P. W. Krenn *et al*., ILK induction in lymphoid organs by a TNFα-NF-κB-regulated pathway promotes the development of chronic lymphocytic leukemia. *Cancer Res.* **76**, 2186–2196 (2016). doi: 10.1158/0008-5472.CAN-15-3379; pmid: 26837762
36. C. C. Zheng *et al*., Significance of integrin-linked kinase (ILK) in tumorigenesis and its potential implication as a biomarker and therapeutic target for human cancer. *Am. J. Cancer Res.* **9**, 186–197 (2019). pmid: 30755822
37. R. Gabizon *et al*., Efficient targeted degradation via reversible and irreversible covalent PROTACs. *J. Am. Chem. Soc.* **142**, 11734–11742 (2020). doi: 10.1021/jacs.9b13907; pmid: 32369353
38. S. Persad *et al*., Inhibition of integrin-linked kinase (ILK) suppresses activation of protein kinase B/Akt and induces cell cycle arrest and apoptosis of PTEN-mutant prostate cancer cells. *Proc. Natl. Acad. Sci. U.S.A.* **97**, 3207–3212 (2000). doi: 10.1073/pnas.97.7.3207; pmid: 10716737
39. X. Sun *et al*., PROTACs: Great opportunities for academia and industry. *Signal Transduct. Target. Ther.* **4**, 64 (2019). doi: 10.1038/s41392-019-0101-6; pmid: 31885879
40. M. Cippitelli *et al*., Role of Aiolos and Ikaros in the antitumor and immunomodulatory activity of IMiDs in multiple myeloma: Better to lose than to find them. *Int. J. Mol. Sci.* **22**, 1103 (2021). doi: 10.3390/ijms22031103; pmid: 33499314
41. J.-H. Wang *et al*., Aiolos regulates B cell activation and maturation to effector state. *Immunity* **9**, 543–553 (1998). doi: 10.1016/S1074-7613(00)80637-8; pmid: 9806640
42. M. L. Holmes *et al*., Peripheral natural killer cell maturation depends on the transcription factor Aiolos. *EMBO J.* **33**, 2721–2734 (2014). doi: 10.15252/embj.201487900; pmid: 25319415
43. C. Schmitt *et al*., Aiolos and Ikaros: Regulators of lymphocyte development, homeostasis and lymphoproliferation. *Apoptosis* **7**, 277–284 (2002). doi: 10.1023/A:1015372322419; pmid: 11997672
44. E. C. Fink, B. L. Ebert, The novel mechanism of lenalidomide activity. *Blood* **126**, 2366–2369 (2015). doi: 10.1182/blood-2015-07-567958; pmid: 26438514
45. A. Goy *et al*., Ibrutinib plus lenalidomide and rituximab has promising activity in relapsed/refractory non–germinal center B-cell–like DLBCL. *Blood* **134**, 1024–1036 (2019). doi: 10.1182/blood.2018891598; pmid: 31331917
46. B. E. Smith *et al*., Differential PROTAC substrate specificity dictated by orientation of recruited E3 ligase. *Nat. Commun.* **10**, 131 (2019). doi: 10.1038/s41467-018-08027-7; pmid: 30631068
47. X. Zhou, R. Dong, J.-Y. Zhang, X. Zheng, L.-P. Sun, PROTAC: A promising technology for cancer treatment. *Eur. J. Med. Chem.* **203**, 112539 (2020). doi: 10.1016/j.ejmech.2020.112539; pmid: 32698111
48. N. Chopra *et al*., Dynamic allostery mediated by a conserved tryptophan in the Tec family kinases. *PLOS Comput. Biol.* **12**, e1004826 (2016). doi: 10.1371/journal.pcbi.1004826; pmid: 27010561
49. V. Modi, R. L. Dunbrack Jr., Defining a new nomenclature for the structures of active and inactive kinases. *Proc. Natl. Acad. Sci. U.S.A.*

116, 6818–6827 (2019). doi: 10.1073/pnas.1814279116; pmid: 30867294
50. S. S. Taylor, A. P. Kornev, Protein kinases: Evolution of dynamic regulatory proteins. *Trends Biochem. Sci.* **36**, 65–77 (2011). doi: 10.1016/j.tibs.2010.09.006; pmid: 20971646
51. H. S. Meharena *et al*., Decoding the interactions regulating the active state mechanics of eukaryotic protein kinases. *PLOS Biol.* **14**, e2000127 (2016). doi: 10.1371/journal.pbio.2000127; pmid: 27902690
52. M. Hallek *et al*., iwCLL guidelines for diagnosis, indications for treatment, response assessment, and supportive management of CLL. *Blood* **131**, 2745–2760 (2018). doi: 10.1182/blood-2017-09-806398; pmid: 29540348
53. Z. Yao *et al*., Tumours with class 3 BRAF mutants are sensitive to the inhibition of activated RAS. *Nature* **548**, 234–238 (2017). doi: 10.1038/nature23291; pmid: 28783719
54. S. J. Heidorn *et al*., Kinase-dead BRAF and oncogenic RAS cooperate to drive tumor progression through CRAF. *Cell* **140**, 209–221 (2010). doi: 10.1016/j.cell.2009.12.040; pmid: 20141835
55. A. L. Shaffer 3rd *et al*., Overcoming acquired epigenetic resistance to BTK inhibitors. *Blood Cancer Discov.* **2**, 630–647 (2021). doi: 10.1158/2643-3230.BCD-21-0063; pmid: 34778802
56. J. Li *et al*., TMTpro-18plex: The expanded and complete set of TMTpro reagents for sample multiplexing. *J. Proteome Res.* **20**, 2964–2972 (2021). doi: 10.1021/acs.jproteome.1c00168; pmid: 33900084
57. J. Navarrete-Perea, Q. Yu, S. P. Gygi, J. A. Paulo, Streamlined tandem mass tag (SL-TMT) protocol: An efficient strategy for quantitative (phospho)proteome profiling using tandem mass tag-synchronous precursor selection-MS3. *J. Proteome Res.* **17**, 2226–2236 (2018). doi: 10.1021/acs.jproteome.8b00217; pmid: 29734811
58. M. E. Ritchie *et al*., limma powers differential expression analyses for RNA-sequencing and microarray studies. *Nucleic Acids Res.* **43**, e47–e47 (2015). doi: 10.1093/nar/gkv007; pmid: 25605792
59. H. Wickham, *Ggplot2* (Springer, 2011).

ACKNOWLEDGMENTS

We thank T. Shih, A. Schwab, S. Konchada, S. Mutyala, and Z. Wartena for providing clinical trial data. **Funding:** S.Mo. is supported by the Ruth L. Kirschstein National Research Service Award for Individual Predoctoral Fellows (1F31CA275378). J.B. is supported by Fondation de France, Francois Wallace Monahan fellowship, Philippe Foundation, and the MSKCC Society Scholars Prize. R.Q.N. is supported by NIH KL2: NCATS 5KL2TR001865. S.S.S. is supported by the Research Council of Norway under the frames of ERA PerMed (project number 322898) and Digital Life Norway (project number 294916) and by Radiumhospitalets Legater. O.A.-W. is supported in part by the Edward P. Evans Foundation, NIH/NCI (R01 CA251138 and R01 CA242020), NIH/NHLBI (R01 HL128239), NIH/NCI P50 CA254838-01, and the Leukemia & Lymphoma Society. We acknowledge the use of the Integrated Genomics Operation Core and the Gene Editing and Screening Core, funded by the NCI Cancer Center Support Grant (CCSG, P30 CA08748), Cycle for Survival, and the Marie-Josée and Henry R. Kravis Center for Molecular Oncology. J.T. is supported by NCI/NIH (K08CA230319), the Doris Duke Charitable Foundation, the Edward P. Evans Foundation, and the NCI Cancer Center Support Grant (CCSG, P30 CA240139) to Sylvester Comprehensive Cancer Center. **Author contributions:** M.N., H.L., G.M.H., O.A.-W., and J.T. designed the study. S.Mo., J.B., M.N., H.L., A.C., J.J., A.K.S., S.G., Y.S.T., S.Y., A.U., E.W., C.H., X.M., W.J.K., Q.S., P.A., H.B., N.B., B.B., M.G., T.S., C.G., J.N.I., T.K., R.M., P.J.R., J.P., M.S.G.d.I.R., J.Y., C.B.R., D.T., G.P., R.Q.N., A.P., M.A., V.N., T.M.T., C.P.-V., A.L., R.K.S., S.S.S., R.J.B., and A.M. performed laboratory experiments. M.C.T., J.M.R., A.D.Z., A.A., L.E.R., and A.R.M. saw patients and collected clinical data. S.Mo., R.K.S., O.A.-W., and J.T. designed and executed proteomics experiments. S.Me. and R.G., designed and generated inducible knockdown vectors. S.Mo., J.B., M.N., H.L., G.M.H., O.A.-W., and J.T. prepared the manuscript with input from all coauthors. **Competing interests:** J.M.R. has served as a consultant for AbbVie, AstraZeneca, BeiGene, Pharmacyclics, Genentech, TG Therapeutics, and Verastem and has received research funding, unrelated to the current manuscript, from Acerta, Pharmacyclics, Oncternal Pharmaceuticals, AbbVie, VelosBio, and Loxo Oncology. A.A. has received research funding from Loxo Oncology, BeiGene, and Incyte and has served on advisory boards for Kite, Seagen, Epizyme, Janssen, BeiGene, Incyte, TG Therapeutics, Lilly, and Genentech. L.E.R. has served as a consultant for AbbVie, Ascentage, AstraZeneca, BeiGene, Janssen, Loxo Oncology, Pharmacyclics, Pfizer, and TG Therapeutics; has served as a continuing medical education speaker for DAVA, Curio, Medscape, and PeerView; holds minority ownership interest in Abbott Laboratories; received travel support from Loxo Oncology; and has received research funding (paid to the institution) from Adaptive Biotechnologies, AstraZeneca, Genentech, AbbVie, Pfizer, Loxo Oncology, Aptose Biosciences, Dren Bio, and Qilu Puget Sound Biotherapeutics. S.S.S. has received honoraria from AbbVie and AstraZeneca and research support from BeiGene and TG Therapeutics outside of this work. O.A.-W. has served as a consultant for H3 Biomedicine, Foundation Medicine Inc., Merck, Prelude Therapeutics, and Janssen and is on the scientific advisory board of Envisagenics Inc., AIChemy, Harmonic Discovery Inc., and Pfizer Boulder. O.A.-W. has received prior research funding, unrelated to the current manuscript, from H3 Biomedicine, Nurix Therapeutics, Minovia Therapeutics, and Loxo Oncology. O.A.-W. is a founder of Codify Therapeutics, where he also serves as a consultant and receives research support. M.N., H.L., S.G., Y.S.T., S.Y., H.B., N.B., B.B., M.G., C.G., J.N.I., T.K., R.M., J.P., M.S.G.d.I.R., J.Y., R.J.B., and G.M.H. are employees of Nurix Therapeutics. The remaining authors declare that they have no competing interests. **Data and materials availability:** The mass spectrometry phosphoproteomics data and mass spectrometry IP data have been deposited to the ProteomeXchange Consortium via the PRIDE partner repository with the dataset identifier PXD039012. The data are accessible at this site: https://www.ebi.ac.uk/pride/archive/projects/PXD039012. All other relevant data are included in the manuscript and the supplementary materials.

SUPPLEMENTARY MATERIALS

Submitted 7 May 2023; accepted 8 December 2023
10.1126/science.adi5798